4

Macromechanical analysis of 3-D textile reinforced composites

A. MIRAVETE, R. CLEMENTE AND L. CASTEJON

4.1 Introduction

Both laminated composite materials [1] and 3-D textile reinforced composite materials [2] are characterized by being composed of biphasic materials: fibres and matrices [3]. The macromechanical analysis of 3-D textile reinforced composite materials is defined by the strain–stress relations, the failure modes and the degradation properties from first failure (FF) to last failure (LF) of the material system. Fibre properties and geometry of the fibres [4,5] inside the matrix are considered in the micromechanical analysis, the result being the following macromechanical parameters:

- the strain–stress relations;
- the failure modes;
- degradation properties from first failure to last failure.

The 3-D textile reinforced composite material [6] is no longer considered a biphasic material, but as a system with the properties listed above, as a result of the micromechanical study.

To carry out the macromechanical analysis of a certain complex structure made of 3-D textile reinforced composite materials, the following information is required:

1 The definition of the material models, which will govern the behaviour of the material system in terms of stiffness and strength at a macromechanical level.
2 The introduction of the stiffness and strength properties necessary for the total implementation of the material models of each of the composite systems manufactured by the textile technologies available nowadays.
3 The definition of the geometry of the structure to be analysed, including the geometry of the borders between the different substructures, which can be made by different manufacturing textile technologies.

4 The definition of the boundary of loading conditions, which can be constant or variable with time, owing to the existence of contact or friction conditions from dynamic loads.
5 The design requirements of the structure, object of study.

This information is processed by means of a mathematical model. In most cases, the finite element technique seems to be the most appropriate to solve the numerical problem of obtaining the response of the structure to the loading conditions.

Usually, 1, 3, 4 and 5 are known and 2, which refers to the strength and stress properties, must be either obtained from testing or estimated by means of micromechanical studies. Testing is recommended, when possible, since the accuracy of the results is extremely high when a proper statistical analysis is made. However, in those cases when testing cannot be carried out owing to the high complexity of the characterization, as is the case with some through-thickness normal and transverse properties, or for other reasons, the estimation of properties by means of micromechanical analyses and the finite element technique or analytical procedures constitutes an alternative method, although it is much less accurate.

4.2 Determination of the stiffness and strength properties of 3-D textile reinforced composite materials

The object of the macromechanical analysis is the mechanical prediction of structures made of 3-D textile reinforced composite materials, under given working conditions. The implementation of appropriate material models, simulating the behaviour of the material system under given working conditions, is necessary to carry out this type of analysis.

In order to define the material model properly, simulating the behaviour of the material system, the introduction of a number of stiffness and strength properties is required. However, the material model varies as a function of the following issues:

- type of macromechanical analysis;
- type of theory;
- type of 3-D textile technology.

Owing to the fact that the textile technologies present differences in terms of the type of construction [7], the stiffness and strength properties will also vary in terms of the textile technology used.

The type of macromechanical analysis also affects the material model to be used, and therefore the stiffness and strength properties needed to carry

out the analysis. These parameters will be a function of the type of analysis; linear/non-linear, static or dynamic [8,9], stress or displacement-based, hygrothermal, buckling, modal, crash analysis [10], etc.

Finally, the elastic and strength properties needed also depend on the theory on which the analysis is based.

4.2.1 Theories used for the macromechanical analysis of 3-D textile reinforced composite materials

In this section, several theories applicable to the macromechanical analysis of 3-D textile reinforced composite materials are described. The textile technologies studied correspond to those composite materials constituted by preforms generated from 3-D textiles and those joined by means of the stitching technology. The stiffness properties needed are also analysed.

The most appropriate theories for analysing every textile technology will be selected according to the material typology and the desired degree of accuracy [11].

The classical beam theory

The classical beam theory [11,12] is based on the fourth-order differential equations used in the Euler–Bernoulli bending theory, the torsion and the axial tension–compression theories. The Euler–Bernoulli theory assumes that the transverse section perpendicular to the beam axis remains plane and perpendicular to this axis after deformation. The transverse deflection w is governed by a fourth-order differential equation:

$$\frac{\mathrm{d}^2}{\mathrm{d}x^2}\left(E_x I(x)\frac{\mathrm{d}^2 w}{\mathrm{d}x^2}\right) = f(x) \quad \text{for} \quad 0 < x < L \qquad [4.1]$$

where $f(x)$ is the transverse distributed load, E_x is the elasticity modules in the beam axis direction (x), and $I(x)$ is the inertia momentum as a function of the x-direction. A scheme of these variables is represented in Figs. 4.1 and 4.2.

The following stiffness properties are needed when using the classical beam theory: E_x, G_{xy} and ν_{xy}. The following parameters must also be implemented: $I(x)$, $I_O(x)$, $A(x)$, $A_C(x)$, $k_1(x, y, z)$ and $k_2(x, y, z)$, where: $I(x)$ is inertia momentum, $I_O(x)$ is torsion inertia momentum, $A(x)$ is cross-sectional area, $A_C(x)$ is shear cross-sectional area, $k_1(x, y, z)$ is the function dependent on the cross-sectional shape in position x, used to determine the strain component γ_{xy} and $k_2(x, y, z)$ is the function dependent on the cross-sectional shape in position x, used to determine the strain component γ_{xz}.

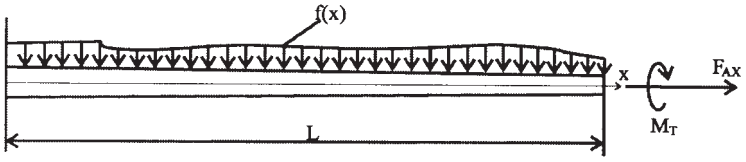

4.1 Scheme of a beam subjected to bending, torsion and tension.

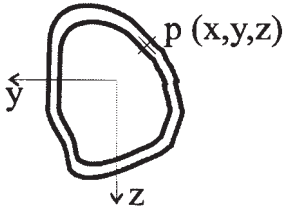

4.2 Scheme of a general cross-section.

Classical laminated plate theory

Nonisotropic and lamination aspects of composite materials are introduced by means of the classical laminated plate theory [2,11,13,14]. This theory takes into account in-plane and bending stresses. Interlaminar stresses are not considered, and therefore the application field of this theory is limited to thin plates with small displacements subject to uniform loads. Those structures subject to impact, free edge effects, stress concentrations, point loads, mechanical and bonded joint, or thick structures are beyond the scope of the classical laminated plate theory.

In terms of order of magnitude, a plate is considered thin when:

$$\frac{\text{plate thickness}}{\text{characteristic length}} < 10 \qquad [4.2]$$

This theory is based on the following assumptions:

- linear variations of strains;
- the perpendicular line to the mid-surface remains perpendicular after deformation; i.e. the strains generated by the shear forces are neglected.

The local axes (x, y, z), the mid-plane x–y and the displacements associated with these axes are represented in Fig. 4.3. The displacement fields are:

$$\begin{aligned} u_x(x,y) &= u(x,y) \\ u_y(x,y) &= v(x,y) \\ u_z(x,y) &= w(x,y) \end{aligned} \qquad [4.3]$$

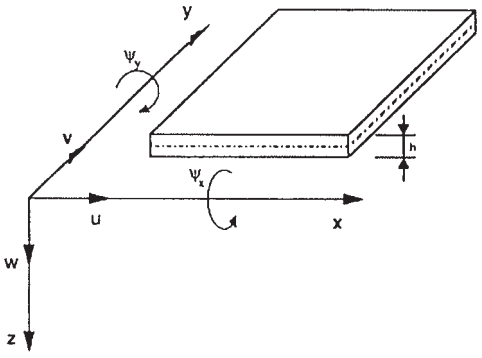

4.3 Definition of a local axis.

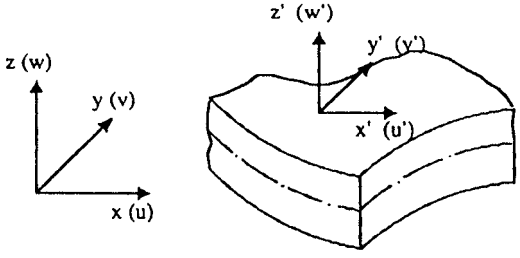

4.4 Definition of plate displacements.

When this theory is applied, the following stiffness properties are needed: E_X, E_Y, G_{XY} and ν_{XY}.

Irons theory

This theory is based on the following assumptions:

- The perpendicular line to the mid-surface of the laminated plate remains straight after deformation.
- The strain energy corresponding to the stresses perpendicular to the mid-surface is neglected.

However, the assumption that the perpendicular line to the mid-surface remains perpendicular after deformation is not imposed. Therefore, interlaminar shear stresses are accounted for in this case. Irons theory considers in-plane and shear stresses for each ply of the laminate.

The relationship between stresses and strains proceeds from a three-dimensional approach. The local axis and the definition of the displacements of the plate are represented in Fig. 4.4. The displacement fields are:

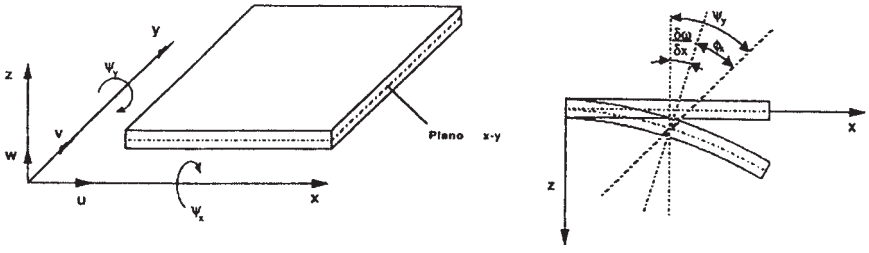

4.5 Displacement field in a thin plate according to YNS theory.

$$u_1(x,y,z) = u(x,y,z)$$
$$u_2(x,y,z) = v(x,y,z) \qquad [4.4]$$
$$u_3(x,y,z) = w(x,y,z)$$

The strain vector is represented in expression 4.5:

$$\varepsilon = [\varepsilon_x, \varepsilon_y, \gamma_{xy}, \gamma_{xz}, \gamma_{yz}] = \left[\frac{\partial u}{\partial x}, \frac{\partial v}{\partial x}, \frac{\partial u}{\partial y} + \frac{\partial v}{\partial x}, \frac{\partial u}{\partial z} + \frac{\partial w}{\partial x}, \frac{\partial v}{\partial y} + \frac{\partial w}{\partial y}\right] \qquad [4.5]$$

The following stiffness properties are needed for this theory: E_X, E_Y, G_{XY}, G_{XZ}, G_{YZ} and v_{XY}.

First-order shear theory

This theory [11] is based on the work from Yang–Norris–Stavsky (YNS), which is a generalization of Mindlin theory to laminated non-isotropic materials. In-plane, bending and shear stresses are accounted for. This theory is applicable to both thin and thick laminated plates, by using an appropriate correction factor.

Figure 4.5 represents a plate with constant thickness h and the parameters needed to define the displacement field. The following equations govern the displacement field by applying YNS theory:

$$u(x,y,z) = u_O(x,y,z) + z\Psi_Y(x,y,z)$$
$$v(x,y,z) = v_O(x,y,z) + z\Psi_X(x,y,z) \qquad [4.6]$$
$$w(x,y,z) = w_O(x,y,z)$$

where: u, v, w = displacement components in the x,y,z directions,
u_O, v_O, w_O = mid-plane linear displacements,
Ψ_X, Ψ_Y = angular displacements around the x,y axes.

The following stiffness properties are needed: E_X, E_Y, G_{XY}, G_{XZ}, G_{YZ} and v_{XY}.

Higher-order shear theory

According to the first-order shear theories, shear strains are constant through the laminate thickness, and therefore they do not satisfy the equilibrium equation at the top and bottom surfaces, where shear strain must be zero if no external force is applied.

For thick laminate plates, an accurate shear strain distribution through the laminate thickness is essential. To satisfy the equilibrium equation above mentioned, a higher-order shear theory must be applied [11,15,16]. In this section, a theory developed by Reddy will be described. In-plane, bending and shear stresses are taken into account, the number of variables being the same as in the first-order shear theories. A parabolic shear strain distribution through the laminate thickness is implemented, the shear strains being zero at both top and bottom surfaces.

The displacement field according to Reddy theory is:

$$\begin{aligned} u(x,y,z) &= u_o(x,y) + z\Psi_y(x,y) + z^2\xi_x(x,y) + z^3\rho_x(x,y) \\ v(x,y,z) &= v_o(x,y) + z\Psi_x(x,y) + z^2\xi_y(x,y) + z^3\rho_y(x,y) \\ w(x,y,z) &= w_o(x,y) \end{aligned} \quad [4.7]$$

where: u_O, v_O, w_O = linear displacements of a point (x,y) at the laminate mid-plane,

Ψ_X, Ψ_Y = angular displacements around the x and y axes,

ξ_X, ξ_Y, ρ_X, ρ_Y = functions to be determined by applying the condition that interlaminar shear stresses must be zero at top and bottom surfaces:

$$\begin{aligned} \sigma_{xz}(x,y,\pm h/2) &= 0 \\ \sigma_{yz}(x,y,\pm h/2) &= 0 \end{aligned} \quad [4.8]$$

The following stiffness properties are needed: E_X, E_Y, G_{XY}, G_{XZ}, G_{YZ} and v_{XY}.

Elasticity theory

The elasticity theory [17] is applicable to both isotropic and non-isotropic materials, owing to the fact that all the effects related to the elasticity are taken into account. This theory is very efficient in those analyses where the whole stress tensor must be considered, including the interlaminar normal or peeling stress. The displacement field is shown in Fig. 4.6.

The strain tensor is given by:

$$\begin{aligned} \varepsilon &= [\varepsilon_x, \varepsilon_y, \varepsilon_z, \gamma_{xy}, \gamma_{xz}, \gamma_{yz}] \\ &= \left[\frac{\partial u}{\partial x}, \frac{\partial v}{\partial y}, \frac{\partial w}{\partial z}, \frac{\partial u}{\partial y} + \frac{\partial v}{\partial x}, \frac{\partial u}{\partial z} + \frac{\partial w}{\partial x}, \frac{\partial v}{\partial y} + \frac{\partial w}{\partial y}\right] \end{aligned} \quad [4.9]$$

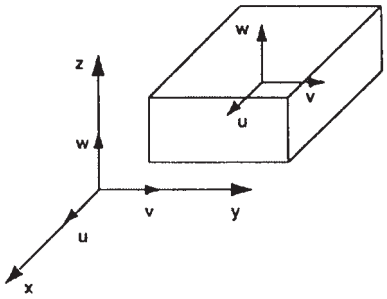

4.6 Displacement field in a thick plate.

Table 4.1. Stiffness properties as a function of the theory used

Theory	Needed stiffness properties
Beams theory	E_X, G_{XY} and v_{XY}
Laminated plates theory	E_X, E_Y, G_{XY} and v_{XY}
Irons's theory	E_X, E_Y, G_{XY}, G_{XZ}, G_{YZ} and v_{XY}
First-order shear theory	E_X, E_Y, G_{XY}, G_{XZ}, G_{YZ} and v_{XY}
Higher-order shear theory	E_X, E_Y, G_{XY}, G_{XZ}, G_{YZ} and v_{XY}
Elasticity theory	E_X, E_Y, E_Z, G_{XY}, G_{XZ}, G_{YZ}, ν_{XY}, ν_{XZ} and v_{YZ}

The following stiffness properties are needed: E_X, E_Y, E_Z, G_{XY}, G_{XZ}, G_{YZ}, v_{XY}, v_{XZ} and v_{YZ}.

Table 4.1 represents the stiffness properties needed as a function of the theory applied.

4.2.2 Stiffness and strength properties as a function of the 3-D textile preform

The 3-D textile preform used as a reinforcement for the composite material affects the needed stiffness and strength properties for two reasons [18–23]:

- On the one hand, every 3-D textile technology is associated with one or more theories among the ones described in Section 4.2.1. Each of these theories requires a specific list of stiffness properties for an appropriate implementation.
- On the other hand, every 3-D textile technology requires one or more specific strength criteria and, therefore, a number of strength properties.

In the following sections, the most important 3-D textile technologies will be analysed. Special attention will be paid to the strength criterion for each case.

Braiding

Depending on the type of braiding technology considered (2-D or 3-D), there are several options in terms of type of finite element used and type of theory applied. This issue is analysed in Table 4.2. The most appropriate failure criterion for static analyses of braided preforms is the 3-D Tsai–Wu criterion [1]. For dynamic studies, the maximum strain criterion gives very interesting results until the final failure occurs.

For those studies where out-of-plane stresses must be considered, the introduction of interaction factors between normal and shear stress components in the 3-D Tsai–Wu criterion generates more accurate results. In this case, the general quadratic criterion to be applied is governed by the following equations:

$$F_{ij}\sigma_{ij} + F_i\sigma_{ii} = 0 \quad i, j = 1 \div 6 \qquad \text{(criterion 1)}$$

where:

$$F_1 = \frac{1}{X} - \frac{1}{X'} \quad F_2 = \frac{1}{Y} - \frac{1}{Y'} \quad F_3 = \frac{1}{Z} - \frac{1}{Z'} \quad F_4 = F_5 = F_6 = 0$$

$$F_{11} = \frac{1}{XX'} \quad F_{22} = \frac{1}{YY'} \quad F_{33} = \frac{1}{ZZ'} \qquad [4.10]$$

$$F_{44} = \frac{1}{S^2_{xy}} \quad F_{55} = \frac{1}{S^2_{xz}} \quad F_{66} = \frac{1}{S^2_{yz}}$$

$$F_{45} = F_{46} = F_{56} = 0 \quad F_{ij} = -0.5\sqrt{F_{ii}F_{jj}} \quad i, j = 1 \div 6 \text{ and } i \neq j$$

When other theories on general elasticity are applied, the stress tensor is considerably reduced:

- For beam theory, the stress tensor is composed of σ_x and τ_{xy}, and therefore the criterion can be simplified to the following expression:

$$F_{11}\sigma_x{}^2 + F_{44}\tau_{xy}{}^2 + F_1\sigma_x + 2F_{14}\sigma x\tau_{xy} = 1 \qquad \text{(criterion 2) [4.11]}$$

- For the classical laminated plate theory, the stress components are σ_x, σ_y and τ_{xy}, and the failure criterion corresponds to:

$$F_{11}\sigma_x{}^2 + F_{22}\sigma_y{}^2 + F_{44}\tau_{xy}{}^2 + F_1\sigma_x + F_2\sigma_y + 2F_{12}\sigma_x\sigma_y + 2F_{14}\sigma_x\tau_{xy} + 2F_{24}\sigma_y\tau_{xy} = 1 \qquad \text{(criterion 3) [4.12]}$$

Table 4.2. Properties to be applied as a function of the type of braiding technology

Type of braiding	Type of element	Theory implemented	Requested stiffness properties	Requested strength properties	Strength criterion
2-D	Beam	Unidimensional	E_X, G_{XY} and v_{XY}	X, X' and S_{xy}	Criterion 2
2-D	Shell	Laminated plates theory	E_X, E_Y, G_{XY} and v_{XY}	X, X', Y, Y' and S_{XY}	Criterion 3
2-D	Shell	Irons's theory	E_X, E_Y, G_{XY}, G_{XZ}, G_{YZ} and v_{XY}	X, X', Y, Y', S_{xy} S_{xz} and S_{yz}	Criterion 4
2-D	Shell	First-order shear theory	E_X, E_Y, G_{XY}, G_{XZ}, G_{YZ} and v_{XY}	X, X', Y, Y', S_{xy} S_{xz} and S_{yz}	Criterion 4
2-D	Shell	Higher-order shear theory	E_X, E_Y, G_{XY}, G_{XZ}, G_{YZ} and v_{XY}	X, X', Y, Y', S_{xy} S_{xz} and S_{yz}	Criterion 4
2-D	Solid	Elasticity theory	E_X, E_Y, E_Z, G_{XY}, G_{XZ}, G_{YZ}, v_{XY}, v_{XZ} and v_{YZ}	X, X', Y, Y', Z, Z', S_{xy} S_{xz} and S_{yz}	Criterion 1
3-D	Beam	Unidimensional	E_X, G_{XY} and v_{XY}	X, X' and S_{xy}	Criterion 2
3-D	Solid	Elasticity theory	E_X, E_Y, E_Z, G_{XY}, G_{XZ}, G_{YZ}, v_{XY}, v_{XZ} and v_{YZ}	X, X', Y, Y', Z, Z', S_{xy} S_{xz} and S_{yz}	Criterion 1

- When Irons's first- or higher-order shear theories are applied, the stress components are σ_x, σ_y, τ_{xy}, τ_{xz} and τ_{yz} and thus the failure criterion is represented by the following expression:

$$\begin{aligned} &F_{11}\sigma_x^2 + F_{22}\sigma_y^2 + F_{44}\tau_{xy}^2 + F_{55}\tau_{xz}^2 + F_{66}\tau_{yz}^2 \\ &\quad + F_1\sigma_x + F_2\sigma_y + 2F_{12}\sigma_x\sigma_y + 2F_{14}\sigma_x\tau_{xy} \\ &\quad + 2F_{15}\sigma_x\tau_{xz} + 2F_{16}\sigma_x\tau_{yz} + 2F_{24}\sigma_y\tau_{xy} \\ &\quad + 2F_{25}\sigma_y\tau_{xz} + 2F_{26}\sigma_y\tau_{yz} = 1 \end{aligned} \qquad \text{(criterion 4)} \quad [4.13]$$

Table 4.2 shows the type of finite element, theory, needed stiffness and strength properties and failure criterion to be applied depending on the type of braiding technology used.

3-D weaving

The models to be carried out for simulations of 3-D weaving preforms can be constituted by shell or solid finite elements. The most appropriate failure criterion seems to be the 3-D Tsai–Wu criterion, implementing interaction factors between normal and shear stresses. This criterion can be simplified (criteria 2, 3 and 4) should theories different from the one based on elasticity be applied.

Table 4.3 shows the type of finite element, theory, needed stiffness and strength properties and failure criterion to be applied depending on the type of braiding technology used.

Weft knitting

The analysis for the weft knitting technology coincides with the study for 3-D weaving. The models to be carried out for simulations of the weft knitting can be constituted by shell or solid finite elements. The most appropriate failure criterion seems to be the 3-D Tsai–Wu criterion, implementing interaction factors between normal and shear stresses. This criterion can be simplified (criteria 2, 3 and 4) should theories different from the one based on elasticity be applied.

Table 4.4 shows the type of finite element, needed stiffness and strength properties and failure criterion to be applied as a function of the type of theory used.

Warp knitting

Several options exist in terms of type of finite element and theory to be applied, depending on the kind of warp knitted composite material studied (Tables 4.5 and 4.6). When using plain warp knitting [24–26] the treatment is similar to the one described for weft knitting. However, if a

Table 4.3. Properties to be applied as a function of the type of braiding technology

Type of element	Theory	Requested stiffness properties	Requested strength properties	Strength criterion
Shell	Laminated plates theory	E_X, E_Y, G_{XY} and v_{XY}	X, X', Y, Y' and S_{xy}	Criterion 3
Shell	Irons's theory	E_X, E_Y, G_{XY}, G_{XZ}, G_{YZ} and v_{XY}	X, X', Y, Y', S_{xy} S_{xz} and S_{yz}	Criterion 4
Shell	First-order shear theory	E_X, E_Y, G_{XY}, G_{XZ}, G_{YZ} and v_{XY}	X, X', Y, Y', S_{xy} S_{xz} and S_{yz}	Criterion 4
Shell	Higher-order shear theory	E_X, E_Y, G_{XY}, G_{XZ}, G_{YZ} and v_{XY}	X, X', Y, Y', S_{xy} S_{xz} and S_{yz}	Criterion 4
Solid	Elasticity theory	E_X, E_Y, E_Z, G_{XY}, G_{XZ}, G_{YZ}, v_{XY}, v_{XZ} and v_{YZ}	X, X', Y, Y', Z, Z', S_{xy} S_{xz} and S_{yz}	Criterion 1

Table 4.4. Properties to be applied as a function of the theory used

Type of element	Theory	Requested stiffness properties	Requested strength properties	Strength criterion
Shell	Laminated plates theory	E_X, E_Y, G_{XY} and v_{XY}	X, X', Y, Y' and S_{xy}	Criterion 3
Shell	Irons's theory	E_X, E_Y, G_{XY}, G_{XZ}, G_{YZ} and v_{XY}	X, X', Y, Y', S_{xy} S_{xz} and S_{yz}	Criterion 4
Shell	First-order shear theory	E_X, E_Y, G_{XY}, G_{XZ}, G_{YZ} and v_{XY}	X, X', Y, Y', S_{xy} S_{xz} and S_{yz}	Criterion 4
Shell	Higher-order shear theory	E_X, E_Y, G_{XY}, G_{XZ}, G_{YZ} and v_{XY}	X, X', Y, Y', S_{xy} S_{xz} and S_{yz}	Criterion 4
Solid	Elasticity theory	E_X, E_Y, E_Z, G_{XY}, G_{XZ}, G_{YZ}, v_{XY}, v_{XZ} and v_{YZ}	X, X', Y, Y', Z, Z', S_{xy} S_{xz} and S_{yz}	Criterion 1

3-D warp knitted material is studied, there are a number of possibilities, since the sandwich skins can be modelled as a 2-D warp knitted material but the core can be analysed by means of several methods.

The 3-D Tsai–Wu criterion can be applied for analysing 2-D warp knitted materials or the sandwich skins of a 2-D warp knitted system. The interaction factors between normal and shear stresses must be implemented to

Table 4.5 Properties to be applied as a function of the type of theory used for the 2-D warp knitting technology

Type of element	Theory	Requested stiffness properties	Requested strength properties	Strength criterion
Shell	Theory of laminated plates	E_X, E_Y, G_{XY} and v_{XY}	X, X', Y, Y' and S_{xy}	Criterion 3
Shell	Irons's theory	E_X, E_Y, G_{XY}, G_{XZ}, G_{YZ} and v_{XY}	X, X', Y, Y', S_{xy} S_{xz} and S_{yz}	Criterion 4
Shell	First-order shear theory	E_X, E_Y, G_{XY}, G_{XZ}, G_{YZ} and v_{XY}	X, X', Y, Y', S_{xy} S_{xz} and S_{yz}	Criterion 4
Shell	Higher-order shear theory	E_X, E_Y, G_{XY}, G_{XZ}, G_{YZ} and v_{XY}	X, X', Y, Y', S_{xy} S_{xz} and S_{yz}	Criterion 4
Solid	Elasticity theory	E_X, E_Y, E_Z, G_{XY}, G_{XZ}, G_{YZ}, v_{XY}, v_{XZ} and v_{YZ}	X, X', Y, Y', Z, Z', S_{XY} S_{xz} and S_{yz}	Criterion 1

obtain more accurate results. If a theory different from the one based on the elasticity is applied, the number of stress components is drastically reduced, and therefore the expression of the failure criterion becomes more simple (criteria 2, 3 and 4).

The sandwich core is constituted by a pile structure and optionally by a foam. The failure criterion number 5 is considered the most appropriate since shear and peeling stresses are accounted for. Since the pile structure may be different in the two principal directions, the core strength will also vary in both directions.

The expressions of criterion 5 are represented in expression 4.14. There is no peeling failure if:

$$S_{zc}{}^{n} \leq \sigma_z \leq S_{zt}{}^{n}$$

There is no shear failure if:

$$\frac{\tau_{xz}{}^{2}}{S_{xz}{}^{n2}} + \frac{\tau_{yz}{}^{2}}{S_{yz}{}^{n2}} \leq 1 \qquad \text{(criterion 5) [4.14]}$$

where: $S_{zc}{}^{n}$ = core compression strength in the z-direction,
$S_{zt}{}^{n}$ = core tension strength in the z-direction,
$S_{xz}{}^{n}$ = core shear strength in the x–z plane,
$S_{yz}{}^{n}$ = core shear strength in the y–z plane.

Tables 4.5 and 4.6 represent the type of finite element, needed stiffness and strength properties and failure criterion to be applied as a function of

Table 4.6. Properties to be applied as a function of the type of theory used for the 3-D warp knitting sandwich technology

Type of element	Theory	Stiffness properties requested[1]	Strength properties requested[1,2,3]	Strength criterion
Shell including skins and core	Theory of laminated plates	Skins: E_X, E_Y, G_{XY} and v_{XY} Core: E_X^n, E_Y^n, G_{XY}^n and v_{XY}^n	Skins: X, X', Y, Y' and S_{xy} Core: S_{xz}^n and S_{yz}^n	Skins: criterion 3 Core: criterion 5
Shell including skins and core	Irons's theory	Skins: E_X, E_Y, G_{XY}, G_{XZ}, G_{YZ} and v_{XY} Core: E_X^n, E_Y^n, G_{XY}^n, G_{XZ}^n, G_{YZ}^n and v_{XY}^n	Skins: X, X', Y, Y' and S_{xy} Core: S_{xz}^n and S_{yz}^n	Skins: criterion 4 Core: criterion 5
Shell including skins and core	First-order shear theory	Skins: E_X, E_Y, G_{XY}, G_{XZ}, G_{YZ} and v_{XY} Core: E_X^n, E_Y^n, G_{XY}^n, G_{XZ}^n, G_{YZ}^n and v_{XY}^n	Skins: X, X', Y, Y' and S_{xy} Core: S_{xz}^n and S_{yz}^n	Skins: criterion 4 Core: criterion 5
Shell including skins and core	Higher-order shear theory	Skins: E_X, E_Y, G_{XY}, G_{XZ}, G_{YZ} and v_{XY} Core: E_X^n, E_Y^n, G_{XY}^n, G_{XZ}^n, G_{YZ}^n and v_{XY}^n	Skins: X, X', Y, Y' and S_{xy} Core: S_{xz}^n and S_{yz}^n	Skins: criterion 4 Core: criterion 5
Skins: Shell Core: Solid	Skins: theory of laminated plates Core: elasticity theory	Skins: E_X, E_Y, G_{XY} and v_{XY} Core: E_X^n, E_Y^n, E_Z^n, G_{XY}^n, G_{XZ}^n, G_{YZ}^n, v_{XY}^n, v_{XZ}^n and v_{YZ}^n	Skins: X, X', Y, Y' and S_{xy} Core: S_{xz}^n and S_{yz}^n, S_{zC}^n and S_{zT}^n	Skins: criterion 3 Core: criterion 5
Skins: shell Core: solid	Skins: Irons's theory Core: elasticity theory	Skins: E_X, E_Y, G_{XY}, G_{XZ}, G_{YZ} and v_{XY} Core: E_X^n, E_Y^n, E_Z^n, G_{XY}^n, G_{XZ}^n, G_{YZ}^n, v_{XY}^n, v_{XZ}^n and v_{YZ}^n	Skins: X, X', Y, Y' and S_{xy} Core: S_{xz}^n and S_{yz}^n, S_{zC}^n and S_{zT}^n	Skins: criterion 4 Core: criterion 5
Skins: shell Core: solid	Skins: First-order shear theory Core: Elasticity theory	Skins: E_X, E_Y, G_{XY}, G_{XZ}, G_{YZ} and v_{XY} Core: E_X^n, E_Y^n, E_Z^n, G_{XY}^n, G_{XZ}^n, G_{YZ}^n, v_{XY}^n, v_{XZ}^n and v_{YZ}^n	Skins: X, X', Y, Y' and S_{xy} Core: S_{xz}^n and S_{yz}^n, S_{zC}^n and S_{zT}^n	Skins: criterion 4 Core: criterion 5

Table 4.6. (cont.)

Type of element	Theory	Stiffness properties requested[1]	Strength properties requested[1,2,3]	Strength criterion
Skins: shell Core: solid	Skins: higher-order shear theory Core: elasticity theory	Skins: E_X, E_Y, G_{XY}, G_{XZ}, G_{YZ} and v_{XY} Core: E_X^n, E_Y^n, E_Z^n, G_{XY}^n, G_{XZ}^n, G_{YZ}^n, v_{XY}^n, v_{XZ}^n and v_{YZ}^n	Skins: X, X', Y, Y' and S_{xy} Core: S_{xz}^n and S_{yz}^n, S_{zC}^n and S_{zT}^n	Skins: criterion 4 Core: criterion 5
Skins: solid Core: solid	Elasticity theory	Skins: E_X, E_Y, E_Z, G_{XY}, G_{XZ}, G_{YZ}, v_{XY}, v_{XZ} and v_{YZ} Core: E_X^n, E_Y^n, E_Z^n, G_{XY}^n, G_{XZ}^n, G_{YZ}^n, v_{XY}^n, v_{XZ}^n and v_{YZ}^n	Skins: X, X', Y, Y', Z, Z', S_{xy} S_{xz} and S_{yz} Core: S_{xz}^n and S_{yz}^n, S_{zC}^n and S_{zT}^n	Skins: criterion 1 Core: criterion 5
Skins: solid Core: solid Piles: beams	Skins and core: elasticity theory Piles: unidimensional	Skins: E_X, E_Y, E_Z, G_{XY}, G_{XZ}, G_{YZ}, v_{XY}, v_{XZ} and v_{YZ} Core: model of Krieg and Key Piles: E_X^p, G_{XY}^p and v_{XY}^p	Skins: X, X', Y, Y', Z, Z', S_{xy} S_{xz} and S_{yz} Core: S_T, S_C, τ_{max} Piles: σ_{max}^p and τ_{max}^p	Skins: criterion 1 Core: criterion of hydrostatic pressure failure Piles: criterion 2

[1] The superscript$^{(n)}$ indicates that the stiffness and strength properties refer to the sandwich core, and the superscript$^{(p)}$ indicates that the properties refer to the piles.
[2] S_T, S_C, τ_{max} are the tension, compression and shear strengths of the core, respectively.
[3] σ_{max}^p and τ_{max}^p are the maximum tension and shear strengths that the pile fibres can bear.

Table 4.7. Properties to be applied as a function of the type of theory used for the multilayer knitting 4/5-D technology

Type of element	Theory	Requested stiffness properties	Requested strength properties	Strength criterion
Shell	Theory of laminated plates	E_X, E_Y, G_{XY} and v_{XY}	X, X', Y, Y' and S_{xy}	Criterion 3
Shell	Irons's theory	E_X, E_Y, G_{XY}, G_{XZ}, G_{YZ} and v_{XY}	X, X', Y, Y', S_{xy} S_{xz} and S_{yz}	Criterion 4
Shell	First-order shear theory	E_X, E_Y, G_{XY}, G_{XZ}, G_{YZ} and v_{XY}	X, X', Y, Y', S_{xy} S_{xz} and S_{yz}	Criterion 4
Shell	Higher-order shear theory	E_X, E_Y, G_{XY}, G_{XZ}, G_{YZ} and v_{XY}	X, X', Y, Y', S_{xy} S_{xz} and S_{yz}	Criterion 4
Solid	Elasticity theory	E_X, E_Y, E_Z, G_{XY}, G_{XZ}, G_{YZ}, v_{XY}, v_{XZ} and v_{YZ}	X, X', Y, Y', Z, Z', S_{xy} S_{xz} and S_{yz}	Criterion 1

the type of theory used for the 2-D and 3-D warp knitting technologies respectively.

Multilayer knitting 4/5-D

This technology generates textile plane layers, as is the case for 3-D weaving and warp and weft knitted plain techniques. For all these cases, the numerical models to be implemented from multilayer knitting 4/5-D preforms may be constituted by shell or solid elements. There are a number of theories available, with various degrees of accuracy [27].

The 3-D Tsai–Wu criterion can be applied for analysing multilayer knitting 4/5-D technologies. The interaction factors between normal and shear stresses must be implemented to obtain more accurate results. If a theory other than the one based on elasticity is applied, the number of stress components is drastically reduced, and therefore the expression of the failure criterion becomes more simple (criteria 2, 3 and 4).

Table 4.7 shows the type of finite element, needed stiffness and strength properties and failure criterion to be applied as a function of the type of theory used for the multilayer knitting 4/5-D technology.

Stitching

The stitching technology can be differentiated from the other techniques above described, since this is a joint technology and not a process to obtain

textile preforms. However, this technique is essential for joining, from a highly structural point of view, sub-structures manufactured by different preform technologies. Therefore, the analysis of the stitching technique is critical when a macromechanical analysis of a complete structure composed of a number of preformed substructures is carried out [28].

Since the joint area between two preforms by means of a stitching technology is constituted by stitched fibres, this material system can be considered unidirectional. For this case, the Hashin criterion seems to be the most appropriate (criteria 6 and 7):

- Fibre failure: the Hashin criterion takes into account the interaction between compression and shear. The failure of the fibre occurs when one of the following conditions is met:

$$\sigma_x = \sigma_{i\text{ta}} \quad \text{for } \sigma_1 > 0$$

$$\left(\frac{\sigma_1}{\sigma_{i\text{ca}}}\right)^2 + \left(\frac{\tau_{12}^2 + \tau_{13}^2}{\tau_{12\text{sa}}^2}\right)^2 = 1 \quad \text{for } \sigma_1 < 0 \qquad \text{(criterion 6) [4.15]}$$

- Matrix failure: by means of this criterion, the matrix failure occurs when the stresses exceed an interactive combination of normal and maximum shear stresses (criterion 7):

$$\left(\frac{\sigma_n}{\sigma_{2\text{ta}}}\right)^2 + \left(\frac{\tau_{23}^2 + \tau_{13}^2}{\tau_{\text{sa}}^2}\right)^2 = 1 \quad \text{for } \sigma_n < 0$$

$$\left(\frac{\tau_{23}^2 + \tau_{13}^2}{\tau_{\text{sa}}^2}\right)^2 = 1 \quad \text{for } \sigma_n < 0 \qquad \text{(criterion 7) [4.16]}$$

where: $\sigma_{i\text{ca}}$ = allowable compression stress in *i*-direction,
$\sigma_{i\text{ta}}$ = allowable tension stress in *i*-direction,
$\tau_{12\text{sa}}$ = allowable shear stress in the 12-plane,
τ_{sa} = allowable shear stress in the plane perpendicular to the fibres.

In order to assess the stress components in the joint area, it is not necessary to build a finite element mesh of this area, but the stress values in the joint surfaces must be obtained from the finite element mesh of the preformed substructures.

4.3 Determination of the stiffness and strength properties of braided composite materials

An analytical model for the prediction of stiffness and strength properties of 2-D triaxial braided composite materials [29] is presented in this section.

The final properties of the braided material will be a function of the mechanical properties of fibre, matrix and fibre orientations [30]. In order to assess the accuracy of the model presented, a finite element micromechanical model [31], was built. Fibre and matrix were modelled separately [32].

This finite element model for 2-D braiding material can also be used to understand the material behaviour when subjected to different in-plane stresses. This model allows us to obtain information about the stiffness, strength and strain to failure, as well as about the degradation process in the material after the first failure occurs. The analysis focuses on 2-D braiding containing some percentage of 0° orientation fibres, the rest of the fibre having ±α orientations.

4.3.1 Analytical formulation

The following parameters are used in the 2-D braiding analytical predictive expressions:

α = braided fibres orientation
V_0 = 0° fibre volume percentage
V_α = α° fibre volume percentage
$V_f = V_0 + V_\alpha$ = fibre volume percentage
V_m = matrix volume percentage
E_f = Young modulus of fibre
E_m = Young modulus of matrix
ε_{maxf} = strain to failure of fibre
ε_{maxm} = strain to failure of matrix
G_f = shear modulus of fibre
G_m = shear modulus of matrix
γ_{maxm} = angular strain to failure of matrix
ν_m = Poisson coefficient of matrix

E_a, E_b, ε_a, ε_b, dependent stress–strain graphs may be obtained from the analytical formulation, as is shown in Fig. 4.7.

Direction 1

$$E_a = E_f \cos^4\alpha V_\alpha + E_f V_0 + E_m V_m$$

$$E_b = E_f \cos^4\alpha V_\alpha + E_m V_m$$

$$\varepsilon_a = \varepsilon_{maxf}$$

$$\varepsilon_b = \varepsilon_{maxf}/\cos^2\alpha$$

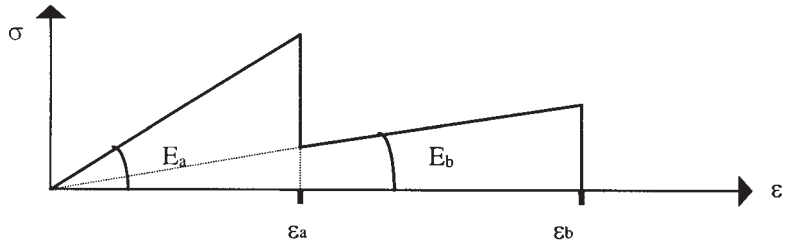

4.7 Parameters obtained from analytical formulation.

Direction 2

$$E_a = E_f \sin^4 \alpha V\alpha + \frac{E_f E_m (V_m + V_0)}{E_f V'_m + E_m V'_0}$$

$$V'_m = \frac{V_m}{V_m + V_0}$$

$$V'_0 = \frac{V_0}{V_m + V_0}$$

$$E_b = \frac{E_f E_m (V_m + V_0)}{E_f V'_m + E_m V'_0}$$

$$\varepsilon_a = \varepsilon_{maxf} / \sin^2 \alpha$$

$$\varepsilon_b = \varepsilon_{maxm}$$

Figures 4.8 and 4.9 show the parameters obtained from an analytical formulation on directions 1 and 2.

In-plane 1–2 shear stress

$$G_a = E_f \sin^2 \alpha \cos^2 \alpha V\alpha + \frac{G_f G_m (V_m + V_0)}{G_f V'_m + G_m V'_0}$$

$$V'_m = \frac{V_m}{V_m + V_0}$$

$$V'_0 = \frac{V_0}{V_m + V_0}$$

$$G_b = \frac{G_f G_m (V_m + V_0)}{G_f V'_m + G_m V'_0}$$

$$\gamma_a = \frac{\varepsilon_{maxf}}{\sin \alpha \cos \alpha}$$

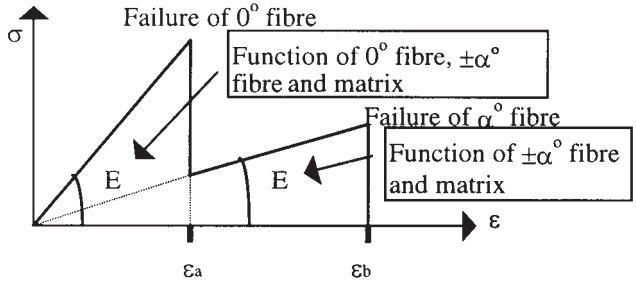

4.8 Parameters obtained from analytical formulation on direction 1.

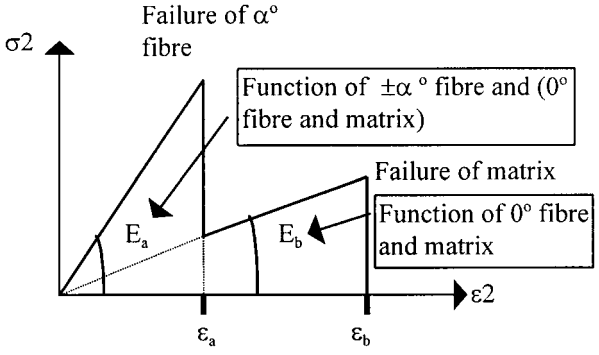

4.9 Parameters obtained from analytical formulation on direction 2.

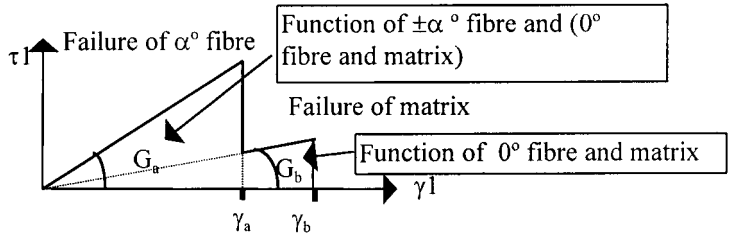

4.10 Parameters obtained from analytical formulation on plane 1–2, shear stress.

$$\gamma_b = \gamma_{maxm} = \frac{\varepsilon_{maxm}(1+\upsilon_m)^2}{\sqrt{3}}$$

Figure 4.10 shows the parameters obtained from an analytical formulation on plane 1–2, shear stress.

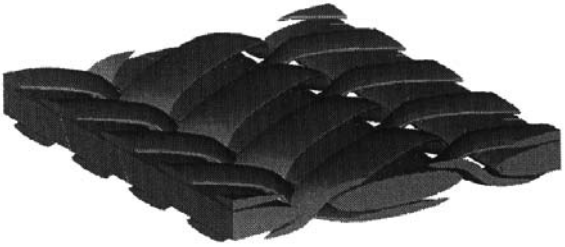

4.11 Fibre model.

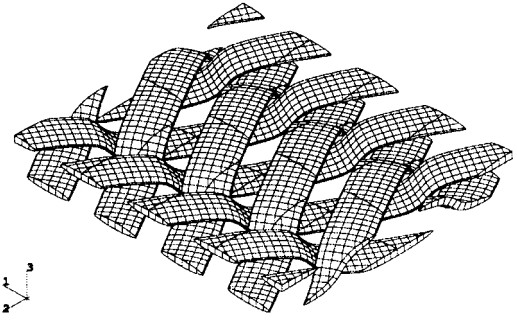

4.12 Finite element model of 60° fibre.

4.3.2 Finite element model for a braided composite $(0°_{65\%}/60°_{35\%})_{V_f=50\%}$

Model properties

The finite element [33] model consists of 14 849 nodes and 24 592 elements classified as follows:

- 8624 eight-node, linear brick, constant pressure, reduced integration, hourglass control elements;
- 2656 six-node linear triangular prism, hybrid, constant pressure elements;
- 13 312 four-node linear tetrahedron elements.

The properties of the 2-D braided material modelled are the following:

$\alpha = 60°$

$V_f = 0.5$

$V_m = 0.5$

$V_{60} = 0.175$

$V_0 = 0.325$

Figures 4.11–4.14 show the finite element model.

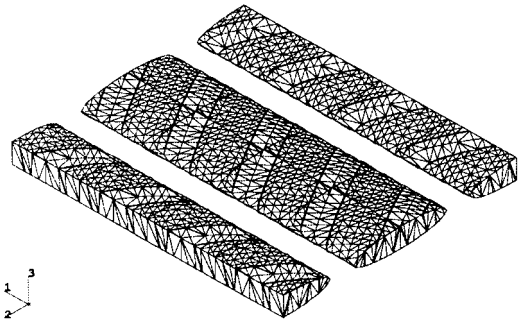

4.13 Finite element model of 0° fibre.

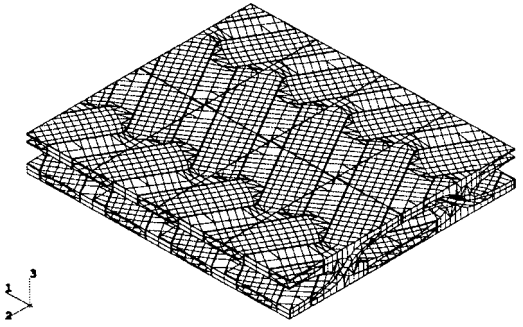

4.14 Finite element model of matrix.

Calculation procedure

Explicit integration procedures were used with Abaqus Explicit 5.6 code [34]. The calculation time is divided into small steps. Some nodes are subjected to different velocities in order to simulate the different stress states. When failure occurs, the material properties are degraded.

Materials

Carbon fibre reinforced epoxy composite was used. The properties of the materials are as follows [35]:

- Carbon fibre:

  Young modulus $E = 250\,\text{GPa}$

  Strength $X = 2700\,\text{MPa}$

  Strain to failure $\varepsilon_r = 1\%$

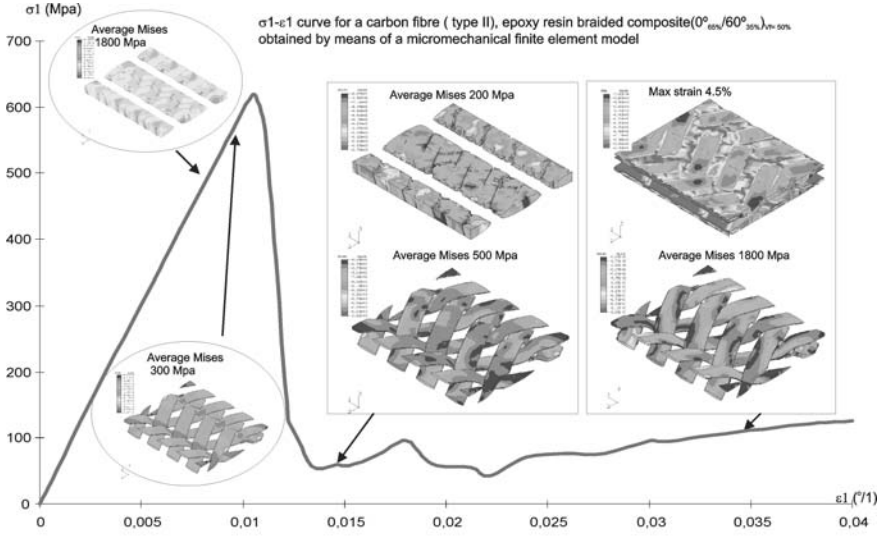

4.15 σ_1–ε_1 curve for a carbon fibre (Type II) epoxy resin braided composite $(0_{65}/60_{35})_{V_f=50\%}$ obtained by means of a micromechanical finite element model.

Table 4.8. Predicted properties

	E_a (GPa)	E_b (GPa)	ε_a (%)	ε_b (%)
Direction 1	85.826	4.626	1	4
Direction 2	29.57	4.96	1.33	4.5
Shear stress in plane 1–2	10.044	1.84	2.3	7.015

- Epoxy resin:

  Young modulus $E = 3.684\,\text{GPa}$

  Strength $X = 123\,\text{MPa}$

  Strain to failure $\varepsilon_r = 4.5\%$

  Poisson coefficient $\nu = 0.35$

Analytical predicted behaviour

The predictive analysis yields the properties given in Table 4.8.

Results

The results of the finite element calculation for a carbon fibre epoxy resin braided composite $(0°_{65\%}/60°_{35\%})_{V_f=50\%}$ can be seen in Figs. 4.15–4.17.

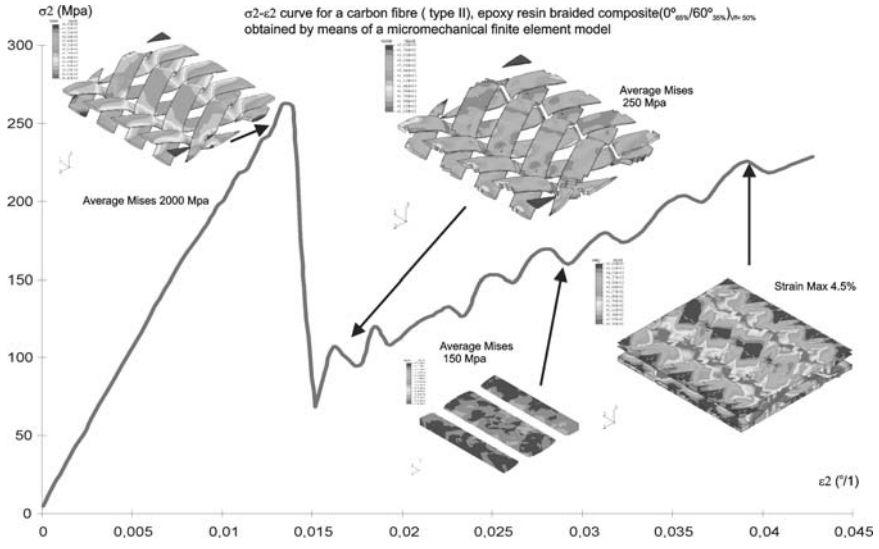

4.16 σ_2–ε_2 curve for a carbon fibre (Type II) epoxy resin braided composite $(0_{65}/60_{35})_{V_f=50\%}$ obtained by means of a micromechanical finite element model.

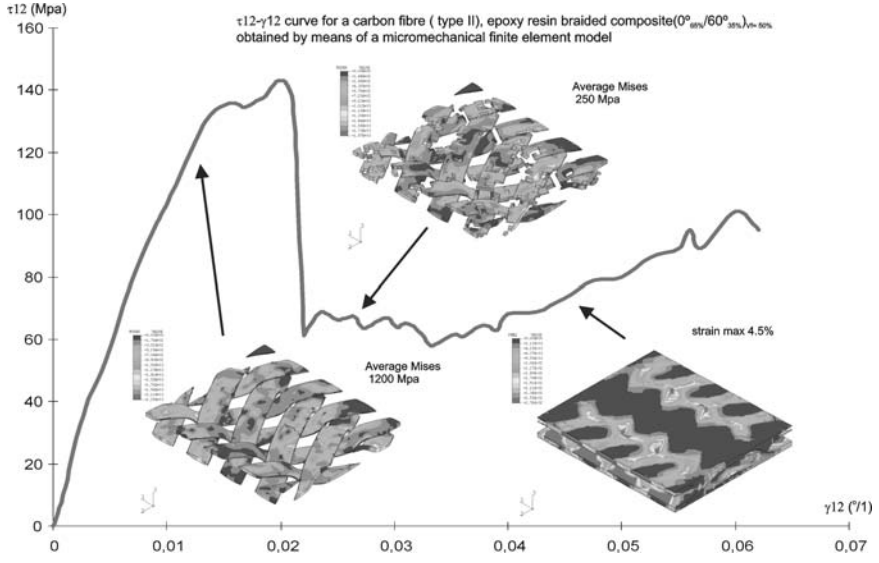

4.17 σ_6–ε_6 curve for a carbon fibre (Type II) epoxy resin braided composite $(0_{65}/60_{35})_{V_f=50\%}$ obtained by means of a micromechanical finite element model.

Low-modulus, high-strength (Type II) carbon fibre reinforced epoxy composite was used, owing to its better ability to absorb deformation energy.

The properties of the material used in the calculation are shown below:

- **Carbon fibre:**

  Young modulus $E = 250\,\text{GPa}$

  Strength $X = 2700\,\text{MPa}$

  Failure strain $\varepsilon_r = 1\%$

4.4 Determination of the stiffness and strength properties of knitted composite materials

The current developments related to weft knitting technology focus on the incorporation of straight fibres to the base fabric in several directions, in order to increase the mechanical properties of the material system. A unit cell of weft knitting is shown in Fig. 4.18. The same cell reinforced with fibres in longitudinal and transverse directions is represented in Fig. 4.19. In this section, the properties of a reinforced weft knitted material will be calculated by means of a finite element micromechanical model [36]. Also, the

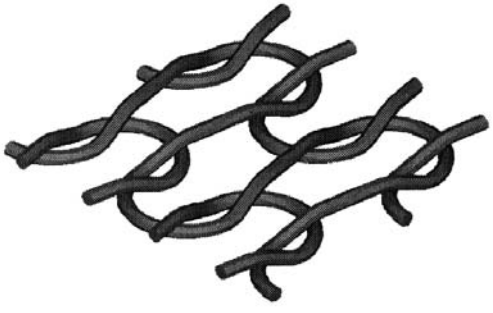

4.18 Weft knitting.

4.19 Reinforced weft knitting.

same weft knitted material without reinforcement will be analysed. The results will be compared with experimental data in order to assess the accuracy of the model used [37].

4.4.1 Model characteristics

Interphase elements have been implemented in the finite element model in order to analyse the starting point of the material failure, where fibres are debonded from the matrix [38–49] or microbuckling phenomena under compression load [42,50–54]. The model used exhibits the following characteristics [37]:

- Fibre fraction volume:

  $V_f = 11\%$ without reinforcement fibres

  $V_f = 17.09\%$ with longitudinal and transverse fibres
- Fibre diameter: 0.238 mm
- Interface thickness: 1.5% of fibre diameter
- Unit cell dimensions are represented in Fig. 4.20.

4.4.2 Materials

The material properties are given in Table 4.9.

4.4.3 Finite element model

The finite element model is composed of 16 000 nodes and 17 464 elements:

- 12 272 eight-node solid linear elements with reduced integration;
- 1824 six-node triangular linear elements;
- 3368 four-node linear tetrahedron elements.

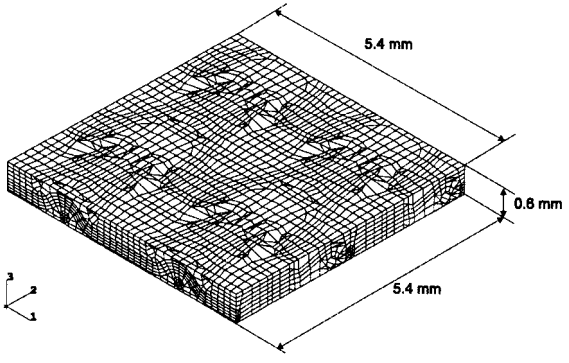

4.20 Dimensions of the unit cell.

Table 4.9. Material properties

	Elastic modulus, E (GPa)	Poisson coefficient, ν	Tension strength, X (MPa)	Strain to failure, $\varepsilon_{failure}$ (%)
E-glass fibre	73	0.24	2336	3.2
Epoxy resin	3.684	0.35	116	6.3
Fibre–matrix interface	3.684	0.35	45	4.5

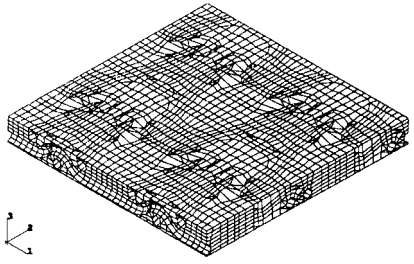

4.21 Resin.

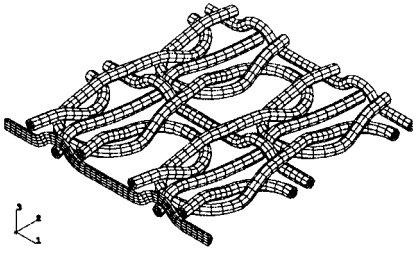

4.22 Fibre.

The elements are divided into three groups according to the material to be modelled (Figs. 4.21–4.23). This model will be used as an example weft-knitted nonreinforced material. In this case, a number of finite elements that modelled the fibre and the interface in the previous case will now pass to model the resin.

Initially, each material is considered to behave in an elastic linear manner. The elastic properties progressively degrade as the deformation increases. When the final failure occurs in a given finite element, that element is removed. Contact has been defined between elements modelling fibre and nodes modelling resin, and between elements modelling fibres. Therefore,

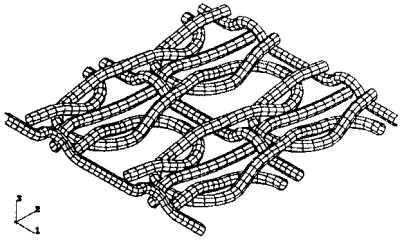

4.23 Fibre–matrix interface.

when an element modelling resin or interface is eliminated, the material is still consistent since the elements modelling the fibres are in contact with the rest of the elements modelling the existing matrix. The following failure modes can be analysed by means of the present model:

- fibre failure;
- matrix failure;
- fibre–matrix interface.

4.4.4 Loading cases and boundary conditions

Nine loading cases have been analysed in order to calculate all the elastic and strength properties of the material system. For each case, velocity has been applied to all the nodes that compose a side of a unit cell. The velocity is linearly increased until a final value of 20 mm/min, then remains constant. An explicit dynamic code has been used to perform this analysis (Abaqus Explicit 5.6) [33].

4.4.5 Results

The stress–strain curve is obtained for each loading case. The average curves for the reinforced weft knitted materials are shown in Fig. 4.24. Directions X, Y and Z correspond to directions 1, 2 and 3. The tension and compression curves in directions X, Y and Z are shown as shear curves in the XY, XZ and YZ planes.

4.4.6 Experiment–theory correlation

Table 4.10 represents the experimental data [37] and the theoretical results obtained by applying the present model for nonreinforced weft-knitted materials. The stiffness and strength properties in tension in X and Y directions are compared, the error being about 1% for the elastic modulus and about 10% for the ultimate tensile strength.

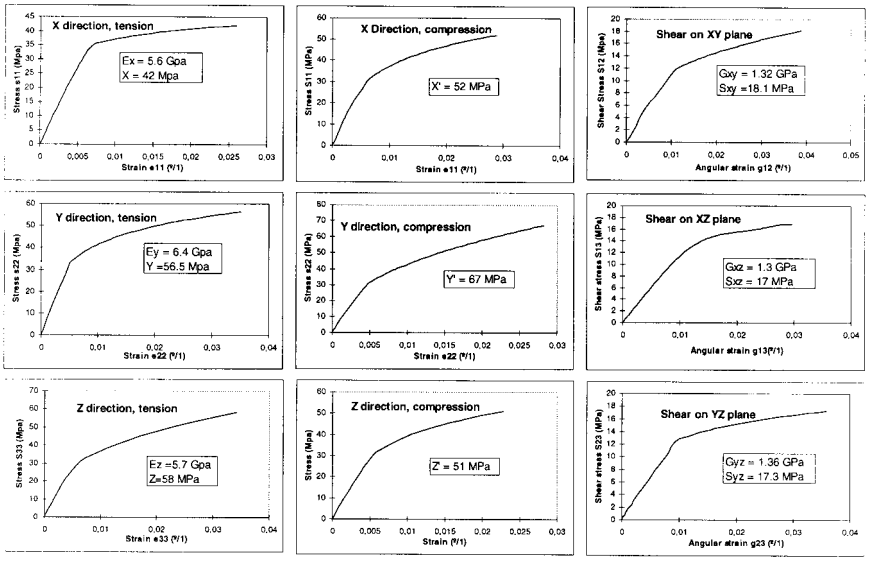

4.24 Stress–strain curves corresponding to knitted composite systems.

Table 4.10. Theory–experiment correlation

	Elastic modulus, *E* (GPa)		Strength, *X* (MPa)		Error (%)	
	Theory	Experiment	Theory	Experiment	*E*	*X*
X-tension	4.331	4.37	40.8	35.5	0.89	13
Y-tension	5.424	5.35	56.93	62.83	1.3	9.3

4.5 Application of macromechanical analysis to the design of a warp knitted fabric sandwich structure for energy absorption applications

A new concept of energy absorber is described in this section. This design can be applied to several air- and ground-transportation means for energy absorption purposes [55–57]. The constitutive materials of the energy absorber, the object of study, are preforms of 3-D warp knitted sandwich structures [58–62].

The macromechanical analysis carried out for the 3-D fabric sandwich structures under given working conditions was essential to design the energy

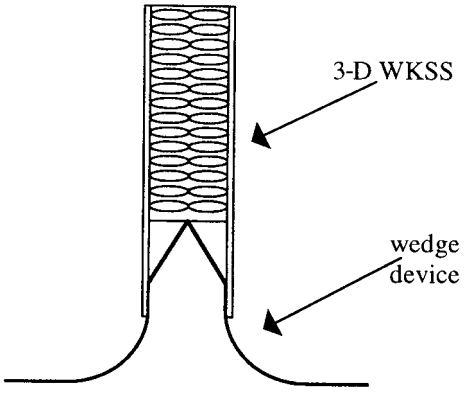

4.25 Concept of energy absorber.

absorber device [58,62]. A numerical–experimental correlation is also shown in order to assess the accuracy of the macromechanical analysis.

4.5.1 Definition of the problem

The concept studied for the energy absorption problem is represented in Fig. 4.25. In a first step, the wedge, which acts as an initial triggering device, attacks the middle part of the 3-D warp knitted sandwich structures (3-D WKSS) and the piles and the foam that compose the core of the sandwich are totally crushed, absorbing a large amount of energy. The failure mechanism of this initial energy absorption mechanism is shear failure.

Once the central part of the 3-D WKSS is destroyed, the skins are pushed against the curved part of the triggering device. By following a bending failure mechanism, the skins are bent and crushed along both sides in a symmetrical way. The geometrical design of the curved part of the triggering device is critical in order to obtain a maximum level of energy absorbed.

Several 3-D warp knitted sandwich panels can be assembled to build a grid showing high performance in terms of energy absorption (Fig. 4.26). This grid can be applied to:

- the undersides of helicopters to absorb the crash energy in case of falling down from a low altitude;
- bus front and lateral parts to absorb the energy generated in the case of a front and roll-over crash, respectively;
- car front parts to absorb front crash energy, etc.

X and T joints between 3-D warp knitted sandwich panels also absorb a large amount of energy and their design is considered essential to obtain an optimum level of energy.

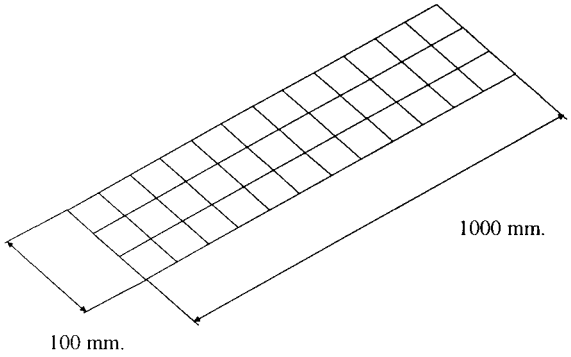

4.26 Absorber energy grid composed of 3-D WKSS.

4.5.2 Requirements for the energy absorption problem

The behaviour of an energy absorption structure must meet the following requirements in terms of the force–displacement curve:

- High energy absorption capability. In other words, the area below the force–displacement curve must be as high as possible.
- The maintained load must be constant along the displacement.
- The initial load peak must be low.
- The maximum displacement must be limited.
- The initial elastic behaviour can be obtained by using an appropriate base structure.
- The specific energy absorption per weight and volume unit must also be high.

An ideal force–displacement curve is represented in Fig. 4.27.

4.5.3 Macromechanical analysis of 3-D warp knitted sandwich panels

A macromechanical analysis of 3-D warp knitted sandwich panels has been carried out. This analysis was dynamic, using an explicit code. The skins were modelled by means of shell finite elements and a higher-order shear theory. The foam was simulated by means of solid elements and elasticity theory and, finally, the piles were modelled by means of beam elements (see Table 4.6). The panels were subjected to a compression load and the force–displacement curve was obtained for the complete crash process. The following data were used:

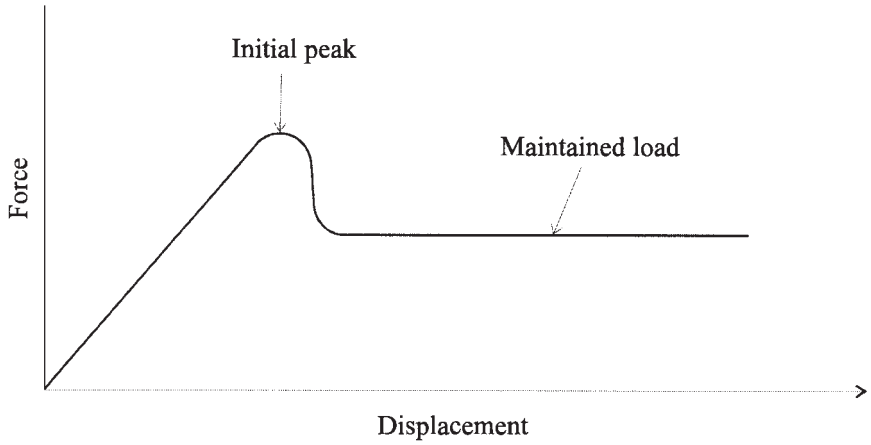

4.27 Ideal force–displacement curve in terms of energy absorption.

- ***Materials***
  - 3-D warp knitted material:
    PARABEAM Ref 89020-1
    Fibre: *E*-glass
    Matrix: epoxy
    Core: polyurethane foam 40 kg/m^3
  - Reinforcing skins:
    Fibres: carbon fibre and aramide
    Matrix: epoxy
    Lay-up:
    Fabric [+45/–45] C/E (0.25 mm)
    Fabric [0/90] C/E (0.25 mm)
    Fabric [+45/–45] A/E (0.25 mm)
- ***Dimensions***

Crash length	75 mm
Height	100 mm
Sandwich thickness	17.5 mm
Core thickness	15 mm
3-D warp knitted skin	
Thickness	0.75 mm
Reinforcing skin thickness	0.5 mm

Two triggering devices were analysed:

- A-type. A sharp wedge-type triggering device for provoking shear failures at an early stage in the material core with curved lateral parts for crushing the sandwich skins (failure mode).

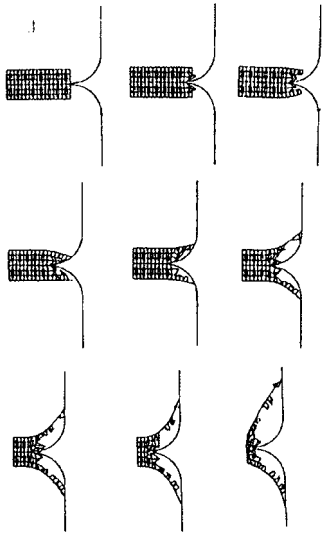

4.28 Series of deformations for the A-type triggering device.

- B-type. A progressive wedge-type triggering device for provoking moderate shear failures in the material core with curved lateral parts for crushing the sandwich skins (failure mode).

A series of deformations along the crash process is represented in Figs. 4.28 and 4.29 for A and B-types, respectively. By comparison of deformations from A and B-type triggering devices, it is observed that type B is more efficient than type A in terms of energy absorption. This is due to the fact that the skins follow the linear device profile before deformation, increasing the energy absorption, the shear failure of the core is more progressive, and therefore the initial peak is lower and the maintained load more constant. The theory–experiment correlation analysis for the B-type triggering device is shown in Fig. 4.30.

The results of the study are outstanding in terms of energy absorption since the initial peak does not exist owing to the fact that the triggering device has been optimized in terms of wedge geometry (shear mode) and curved parts (bending mode). The implementation of a linear profile above the curved part has been essential to eliminate the initial peak. Quite a constant force is also registered along the displacement, the final absorbed energy being excellent compared with other material systems and typologies.

As the wedge penetrates the core with no failure, the value of the force increases up to a point. This phenomenon is represented in Fig. 4.30 by means of a number of increases of the force–displacement curve. These

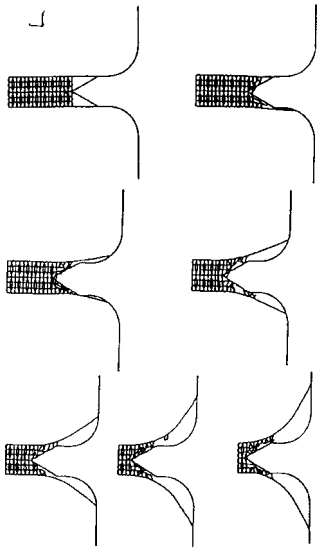

4.29 Series of deformations for the B-type triggering device.

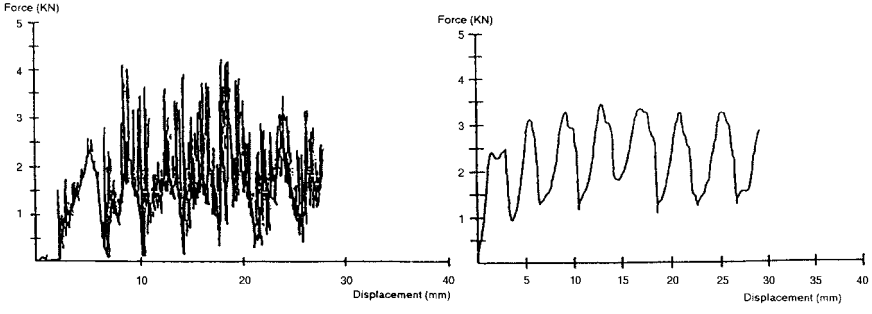

4.30 Comparison between theory (left) and experimentation (right) obtained from the B-type triggering device.

increases generate a number of peaks, which are quite constant along the displacement.

Once the shear failure of the core (piles) occurs, a decrease is observed in the force–displacement curve. A number of shear failures is registered in the curve mentioned. The minima values are also quite constant along the displacement. The progressive core failures are represented by a number of peaks along the displacement. However, these maxima values are quite constant. Finally, the theory–experiment correlation is excellent since the values of the forces are very similar from both studies and the number of increases and decreases registered in the experimental analysis due to the

progressive failure of the piles is very accurately simulated by means of the macromechanical study.

4.5.4 Dynamic macromechanical analysis of X and T joints

A dynamic analysis of the X and T joints has been carried out in order to evaluate the energy absorbed for the whole structure [58,62]. The following data were used:

- ***Materials***
  3-D warp knitted material: PARABEAM Ref 89020-1
  Fibre: *E*-glass
  Matrix: epoxy
  Core: polyurethane foam 40 kg/m^3
- ***Dimensions***

Crash length	75 mm
Height	50 mm
Sandwich thickness	16.4 mm
Core thickness	15 mm
3-D warp knitted skin	
Thickness	0.7 mm

The dimensions are represented in Fig. 4.31.

The progressive deformation of X and T joints is represented in Figs. 4.32 and 4.33. These graphics are the result of a macromechanical study applied to both configurations. The load–displacement curves obtained in the macromechanical analysis are represented in Figs. 4.34 and 4.35.

4.5.5 Conclusions

The main conclusion of this study is that 3-D warp knitted sandwich structures are more efficient than conventional sandwich structures in terms of bending, peeling and crash behaviour, owing to the fact that the connection between the two skins by means of the piles makes this configuration stronger for the cases mentioned above.

4.6 Application of macromechanical analysis to the design of an energy absorber type 3P bending

A material model obtained from Section 4.3 will be used in this section to study the 2-D triaxial braiding technology. A 3P bending dynamic analysis will be performed, considering the material behaviour from the initial step

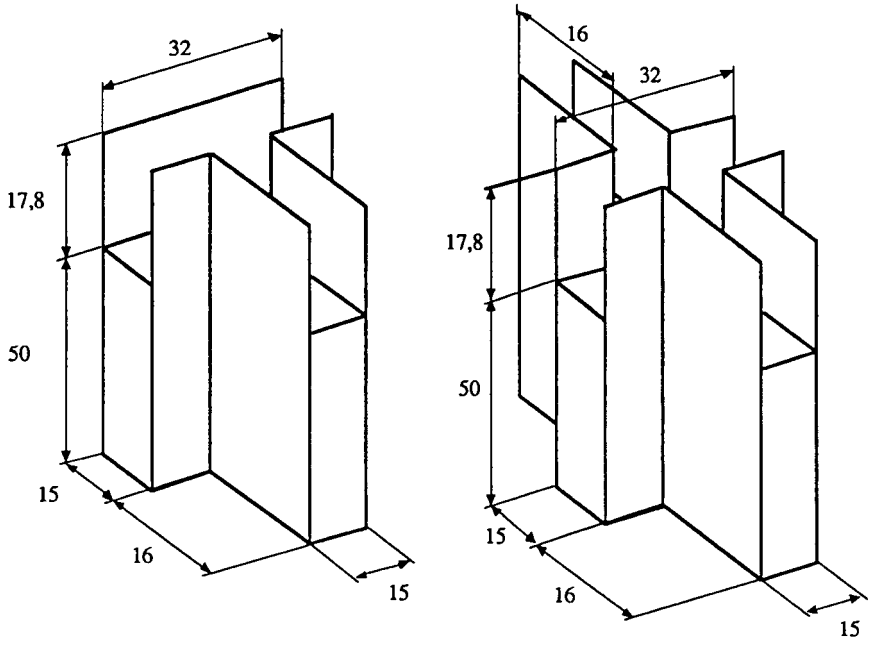

4.31 Dimensions of X and T joints.

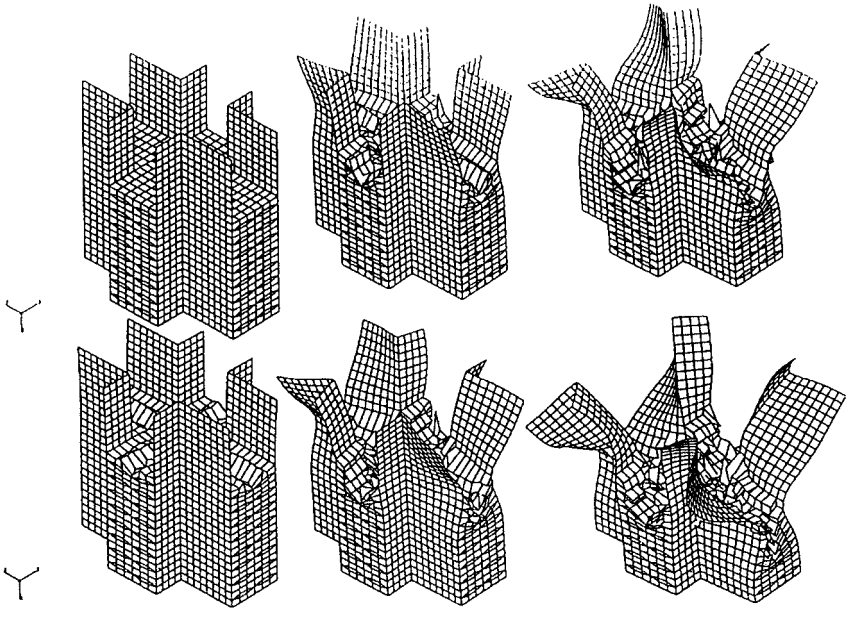

4.32 Progressive deformation of the X joint.

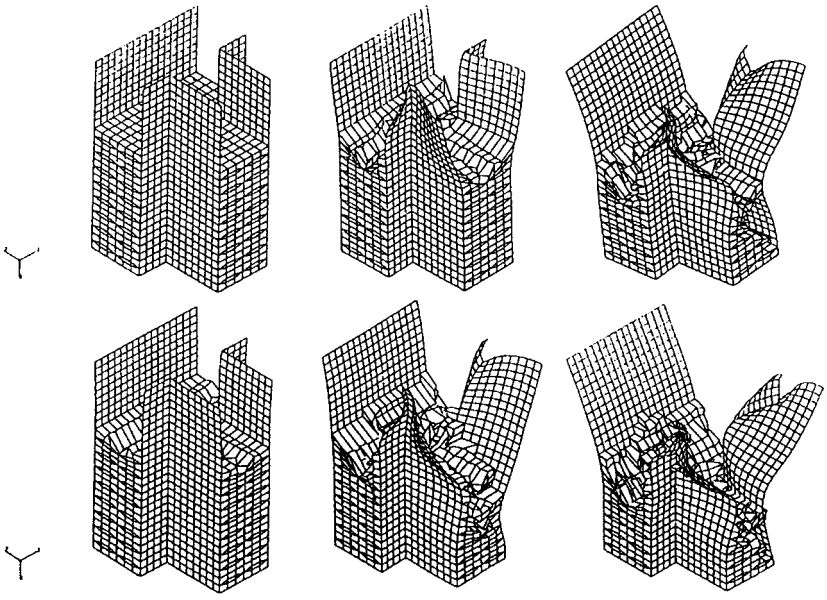

4.33 Progressive deformation of the T joint.

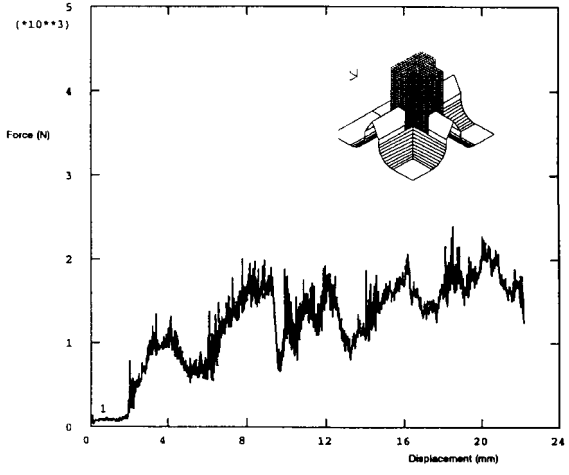

4.34 Force–displacement curve of a T joint.

which is linear and elastic until the final catastrophic failure [63–65]. The aim of this study is to obtain the energy absorbed by a square cross-section beam, subjected to a 3P bending case. Several 2-D braiding and steel configurations will be compared, in terms of energy absorbed, maximum reaction force and weight. This analysis can be considered as a starting point

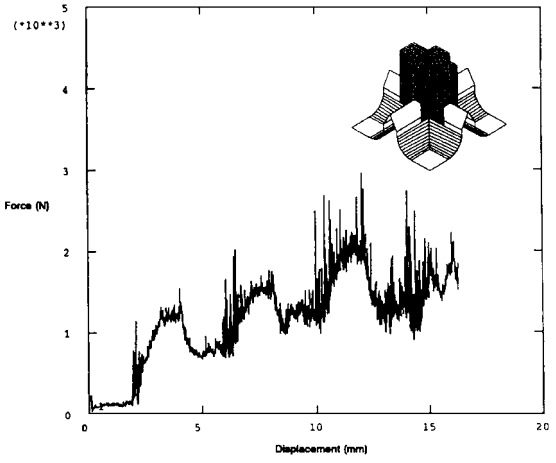

4.35 Force–displacement curve of an X joint.

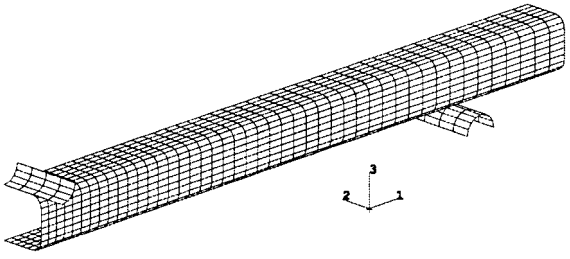

4.36 Finite element model.

for the materials selection in the front crash design of an automotive vehicle [66,67].

4.6.1 Finite element model and boundary conditions

The finite element model used in this study, composed of shell elements, is shown in Fig. 4.36. This model consists of a quarter of the beam, owing to the double symmetry of the problem. The problem, the object of the study, is shown in Fig. 4.37, in which the beam is supported on two rigid cylinders. The load is applied by means of a third rigid cylinder at the middle of the span. Velocity has been imposed in this cylinder, as can be seen in Fig. 4.36.

This problem will be analysed by means of an explicit integration procedure. Contact between the surfaces of the cylinders and the beam has been defined. The material model for 2-D braiding has been introduced by means

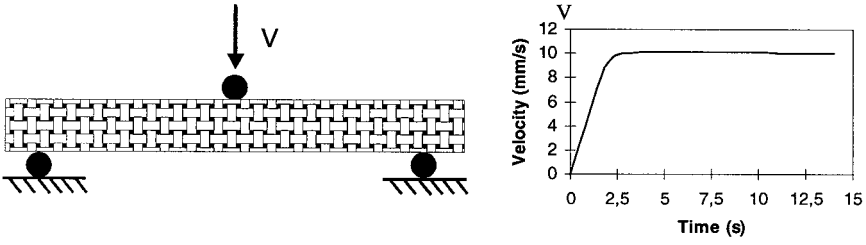

4.37 Three-point bending.

of a Fortran subroutine into the commercial finite element code (Abaqus explicit 5.6) [34].

4.6.2 Configurations analysed

Four different material configurations have been analysed:

1 Steel configuration used as a reference.
2 Carbon fibre–epoxy resin braided configuration $(0°_{50\%}/45°_{50\%})_{V_f=50\%}$. A braided composite material has been considered, constituted by 50% of the fibre oriented along the 1 direction and the other 50% oriented at 45°. Total fibre volume is 50%.
3 Glass fibre–epoxy resin braided composite $(0°_{50\%}/45°_{50\%})_{V_f=50\%}$. In this case, the braided composite material considered is composed of 50% of the fibre oriented along the 1 direction and the other 50% oriented at 45°. Total fibre volume is 50%.
4 Hybrid carbon–aramide fibre–epoxy resin braided composite [65] $(0°_{50\%}/45°_{50\%})_{V_f=50\%}$. Finally, the braided composite material is constituted by 50% of the total fibre in carbon oriented along the 1 direction and the other fibre in aramide oriented with 45°. Total fibre volume is 50%.

The thickness distribution along the beam for every configuration is shown in Fig. 4.38 and Table 4.11.

4.6.3 Materials

The stress–strain curves in the plane of the material are detailed for each material system in this section. These curves have been obtained by applying the analytical formulation described in Section 4.3. The properties of the constitutive materials [35] are the following:

- *Epoxy resin:*

$$E = 3.6\,\text{GPa}$$
$$\nu = 0.38$$
$$\varepsilon_{max} = 4.5\%$$

Table 4.11. Thickness distribution for every configuration

Zone	Thickness (mm) for configuration 1, steel	Thickness (mm) for configuration 2, carbon fibre	Thickness (mm) for configuration 3, glass fibre	Thickness (mm) for configuration 4, hybrid carbon–aramide
A	2	7	5	6
B	2	6	4	5
C	2	5	3	4
D	2	3	3	3

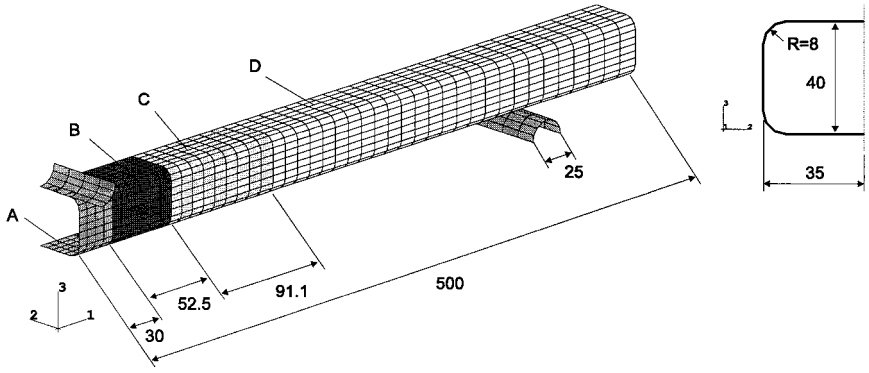

4.38 Zones of the beam.

- *Carbon fibre: PAN Type II (high strength)*

$$E_{II} = 250\,\text{GPa}$$

$$\varepsilon_{II\,max} = 1.08\%$$

$$\sigma_{II\,max} = 2700\,\text{MPa}$$

- *Glass fibre: Type E*

$$E = 76\,\text{GPa}$$

$$\varepsilon_{max} = 3.17\%$$

$$\sigma_{max} = 2400\,\text{MPa}$$

- *Aramide fibre:*

$$E = 133\,\text{GPa}$$

$$\varepsilon_{max} = 2.1\%$$

$$\sigma_{max} = 2800\,\text{MPa}$$

The behaviour of the configurations is shown in Figs. 4.39–4.42.

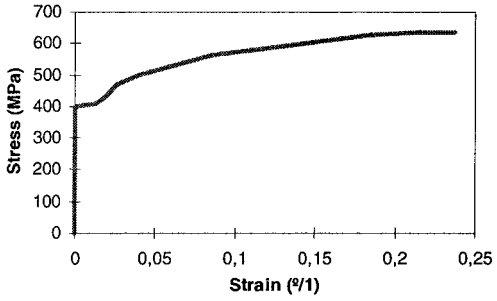

$E = 210$ Gpa

$\nu = 0.3$

4.39 Behaviour of the steel [68].

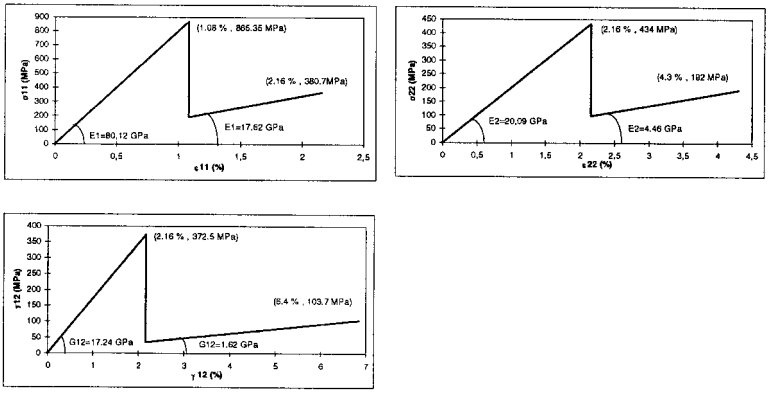

4.40 In-plane stress–strain relationships of carbon configuration.

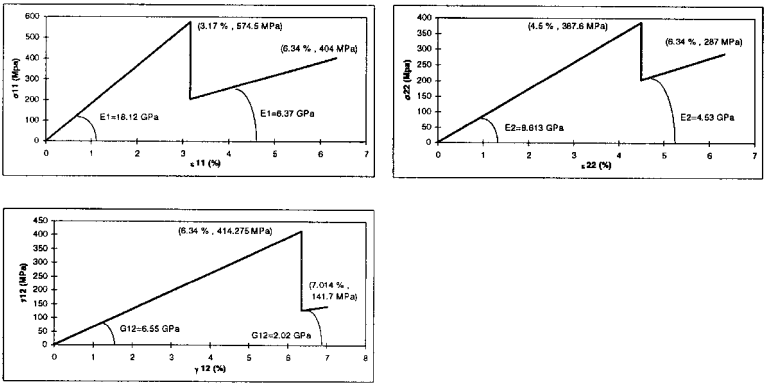

4.41 In-plane stress–strain relationships of glass configuration.

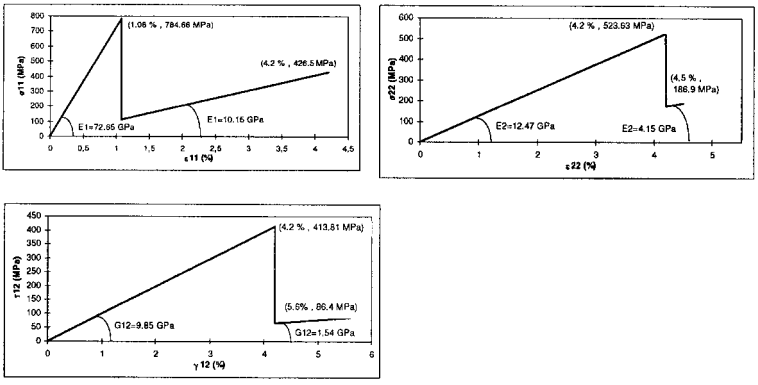

4.42 In-plane stress–strain relationships of hybrid carbon–aramide configuration.

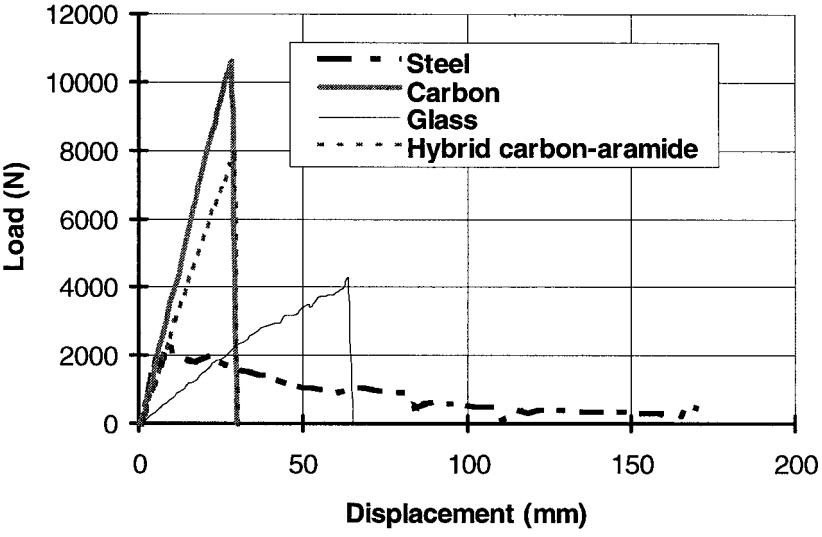

4.43 Load–displacement curves for the configurations calculated.

4.6.4 Results

The curves of the energy absorption versus displacement of the impact cylinder, and reaction force versus displacement of the cylinder are shown in Figs. 4.43 and 4.44. Another important result is the weight of each configuration, and the weight saving obtained (Fig. 4.45). The progressive deformation of the square cross-section beam is represented in Figs. 4.46–4.51.

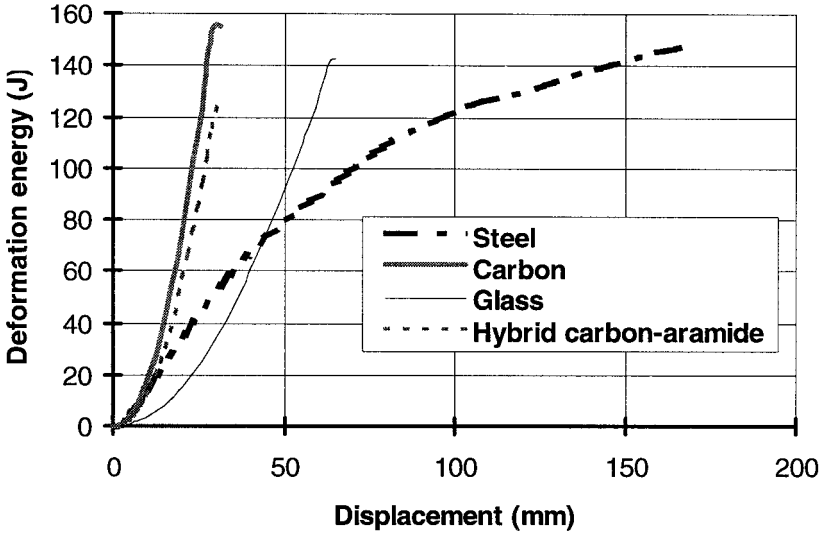

4.44 Deformation energy–displacement curves for the configurations calculated.

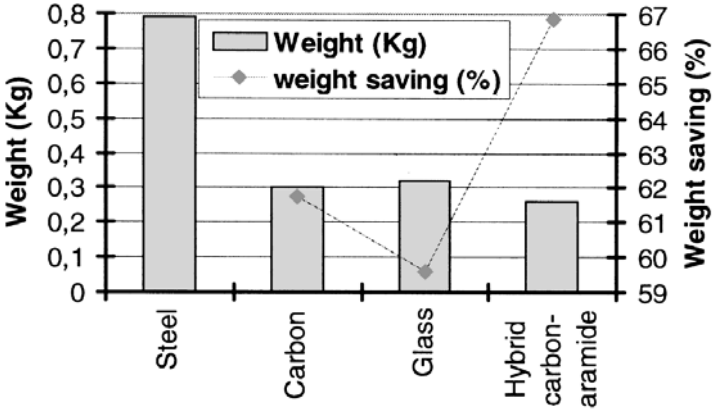

4.45 Weight and weight saving on every configuration.

4.6.5 Conclusions

The energy absorption obtained by using 2-D braided composites subjected to bending is very similar to the energy absorption obtained with steel. The weight saving reported for the braided material is about 60%. This issue is critical for automotive vehicle design, where weight saving is becoming increasingly important, owing to contaminant emission reduction and fuel

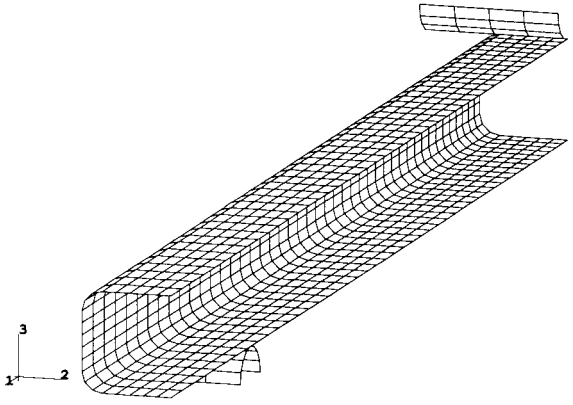

4.46 Deformation for 0 mm displacement at the middle of the span.

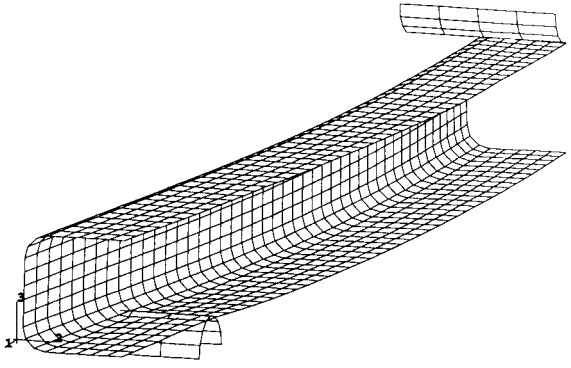

4.47 Deformation for 24.72 mm displacement at the middle of the span.

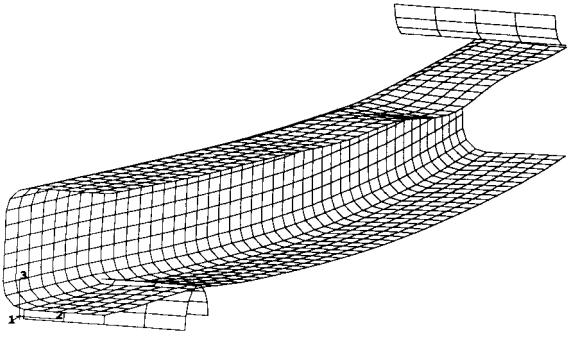

4.48 Deformation for 38.63 mm displacement at the middle of the span.

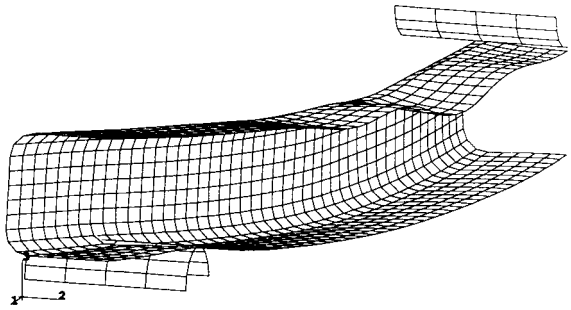

4.49 Deformation for 52.53 mm displacement at the middle of the span.

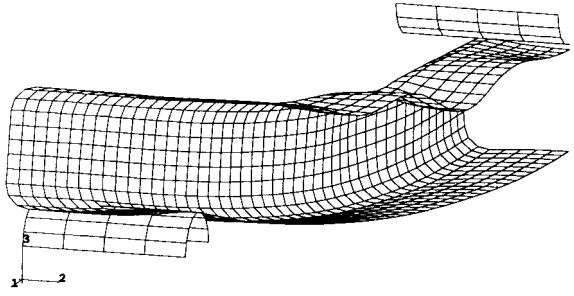

4.50 Deformation for 63.65 mm displacement at the middle of the span.

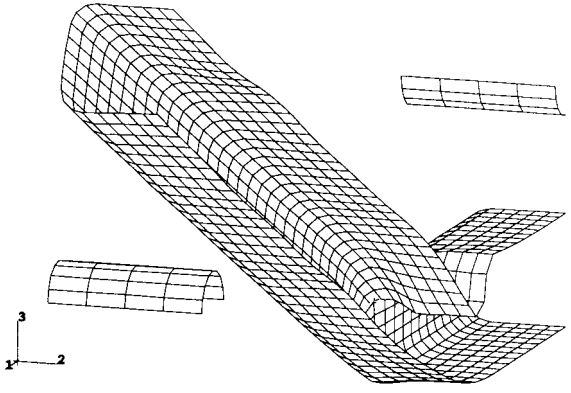

4.51 Deformation for 65 mm displacement at the middle of the span.

consumption saving, and the maximum energy absorbed occurs when the transverse elements break in a bending mode due to a crash impact [69–71].

4.7 Conclusions

Laminated composite materials present some deficiencies, owing to the low out-of-plane properties they exhibit and high manufacturing costs. 3-D textile-reinforced composites are characterized by having their fibres in the thickness direction and being made by means of preforms which can be made automatically. The result is a new generation of composite materials with superior out-of-plane properties, damage tolerance and reasonable manufacturing costs.

Shell and plate finite elements have been used extensively to perform macromechanical analyses of laminated composite materials. Laminated plate and first-order shear theories are being used for thin and thick laminates, respectively.

In order to carry out macromechanical analyses of 3-D textile reinforced composite structures, other theories must also be applied, such as higher-order shear theories, when the interlaminar normal stress component is negligible, or the elasticity theory, which takes into account the whole stress tensor.

Generally speaking, to perform a macromechanical analysis of a given 3-D textile reinforced composite structure, the following information must be known:

- Material models, governing its behaviour in terms of stiffness and strength at a macroscopic level.
- Geometry of the structure.
- Boundary conditions.
- Loading conditions.
- Design requirements.
- Stiffness and strength properties needed, according to the material models defined previously.

All these input data are usually known, except for the last, associated with the stiffness and strength properties. Therefore, the assessment or estimation of these parameters becomes critical for carrying out a macromechanical study of a certain 3-D textile reinforced composite structure.

As has been explained in this chapter, mechanical testing is the best way to evaluate the stiffness and strength properties. However, in some cases, the experimental procedure is not feasible for the determination of certain properties (compression strength, out-of-plane stiffness and strength properties, etc.). In these cases, there are a number of procedures to estimate the properties of the object of study:

- Nowadays, computers are powerful and fast enough to simulate the behaviour of a given 3-D textile reinforced composite material at a fibre level. The estimation of stiffness and strength properties is therefore possible with reasonable precision, by means of the same technology used for macromechanical studies – the finite element method. The interphase can be accurately simulated and the moment of initiation of debonding between fibre and matrix can also be predicted. Non-linear behaviour and contact problems can also be reproduced in order to predict the ultimate strength of the material system. This will let us build the complete curve of the material behaviour in the three directions.
- Several simple analytical formulations exist, which are considered to be approximate, and whose application is usually limited to some in-plane stiffness and strength properties. In any case, the accuracy is very variable.
- Finally, there are also micromechanical studies where more complex analytical formulations are presented.

The stiffness and strength properties needed to carry out a certain macromechanical study depend on the following factors:

- Type of textile technology used.
- Type of macromechanical analysis applied (linear/non-linear, static/dynamic/fatigue/hygrothermal . . .).
- Type of theory implemented.

In this chapter, the factors above outlined have been extensively discussed. Two application examples have also been presented. The finite element method has been applied to two dynamic analyses of 3-D textile reinforced composite structures, taking into account contact problems. The material failure has also been analysed until the final failure occurred.

A theory–experiment correlation study has been carried out, in order to analyse the accuracy of the numerical modelling of a 3-D warp knitted sandwich structure subjected to a crash loading case (dynamic loading, non-linear material and geometry and contact problem). The results of this study have been excellent since both force-displacement curves present very close values.

4.8 References

1. Tsai, S.W., *Theory of Composites Design*, Think Composites, Dayton, Ohio, 1992.
2. Tsai, S.W., Miravete, A. and Diseño, Y., *Análisis De Materiales Compuestos*, Editorial Reverté, SA, Barcelona, 1988.
3. Philips, L.N., *Design with Advanced Composite Materials*, Springer-Verlag, 1989.
4. Vandeurzen, Ph., Ivens, J. and Verpoest, I., 'A three-dimensional micro-

mechanical analysis of woven-fabric composites I. Geometric analysis', *Composites Sci. Technol.*, **56**(11), 1303–1315, 1996.
5. Wood, K. and Whitcomb, J.D., 'Effects of fiber tow misalignment on the engineering properties of plain weave textile composites', *Composite Structures*, **37**(3/4), 343–356, 1997.
6. Bogdanovich, A.E. and Pastore, C.M., *Mechanics of Textile and Laminated Composites with Applications to Structural Analysis*, Chapman & Hall, 1996.
7. Chou, S. and Chen, H.-E., 'The weaving methods of three-dimensional fabrics of advanced composite materials', *Composite Structures*, **33**(3), 159–172, 1995.
8. Reifsnider, K.L., *Fatigue of Composite Materials*, Composite Materials Series, Volume 4, Elsevier, Amsterdam, 1991.
9. Friedrich, K., *Application of Fracture Mechanics to Composite Materials*, Composite Materials Series, Volume 6, Elsevier, Amsterdam, 1990.
10. Lagace, P.A. (Ed.), *Fatigue and Fracture*, Composite Materials series, Volume 2, ASTM, 1989.
11. Reddy, J.N., *Mechanics of Laminated Composite Plates Theory and Analysis*, CRC Press, Boca Raton, 1996.
12. Livesley, R.K., *Matrix Methods of Structural Applications*, Pergamon Press, Oxford, 1978.
13. Jones, R.M., *Mechanics of Composite Materials*, Hemisphere Publishing, 1975.
14. Matthews, F.L. and Rawlings, R.D., *Composite Materials: Engineering and Science*, Chapman & Hall, Oxford, 1994.
15. Gaudenzi, P., 'A general formulation of high order theories for the analysis of laminated plates', *Composite Structures*, **20**(2), 103–112, 1992.
16. Cho, M. and Parmerter, R.R., 'An efficient higher order plate theory for laminated composites', *Composite Structures*, **20**(2), 113–124, 1992.
17. Bhimaraddi, A. and Chandrashekhara, K., 'Three dimensional elasticity solution for static response of simply supported orthotropic cylindrical shells', *Composite Structures*, **20**(4), 227–236, 1992.
18. *Composite Structures*, Special Issue, 'Computer aided mechanical engineering of composite structures', **29**(2), 1994.
19. Alexander, A. and Tzeng, J.T., 'Three dimensional effective properties of composite materials for finite element applications', *J. Composite Mater.*, **31**(5), 466–485, 1997.
20. Naik, N.K. and Ganesh, V.K., 'Failure behavior of plain weave fabric laminates under in-plane shear loading', *J. Composites Technol. Res.*, **16**(1), 3–20, 1994.
21. Naik, N.K., Shembekar, P.S. and Hosur, M.V., 'Failure behavior of woven fabric composites', *J. Composites Technol. Res.*, **13**(2), 107–116, 1991.
22. Hill, B.J., McIlhagger, R. and Abraham, D., *The Design of Textile Reinforcements with Specific Engineering Properties*, Tex Comp 3, New Textiles for Composites, Aachen, 9–11 December, 1996.
23. Mäder, E. and Skop-Cardarella, K., 'Mechanical properties of continuous fibre-reinforced thermoplastics as a function of the textile preform structure', in *The Design of Textile Reinforcements with Specific Engineering Properties*, Hill, B.J., McIlhagger, R. and Abraham, D., eds, Tex Comp 3, New Textiles for Composites, Aachen, 9–11 December, 1996.
24. Ramakrishna, S., Hamada, H., Cuong, N.K. and Maekawa, Z., 'Mechanical properties of knitted fabric reinforced thermoplastic composites', in Proceedings of ICCM-10, Whistler, B.C., Canada, August 1995.

25. Gommers, B. and Verpoest, I., 'Tensile behavior of knitted fabric reinforced composites', in Proceedings of ICCM-10, Whistler, B.C., Canada, August 1995.
26. Huysmans, G., Gommers, B. and Verpoest, I., 'Mechanical properties (2D) warp knitted fabric composites, An experimental and numerical investigation', paper presented at 17th Int. Sampe Europe Conference, Basel, Switzerland, May 1996.
27. Frederiksen, P.S., 'Experimental procedure and results for the identification of elastic constants of thick orthotropic plates', *J. Composite Mater.*, **31**(4), 360–382, 1997.
28. Moll, K. and Wulfhorst, B., 'Determination of stitching as a new method to reinforce composites in the third dimension', in *The Design of Textile Reinforcements with Specific Engineering Properties*, Hill, B.J., McIlhagger, R. and Abraham, D. eds, Tex Comp 3, New Textiles for Composites, Aachen, 9–11 December, 1996.
29. Masters, J.E., Foye, R.L., Pastore, C.M. and Gowayed, Y.A., 'Mechanical properties of triaxial braided composites: experimental and analytical results', *J. Composites Technol. Res.*, **15**(2), 112–122, 1993.
30. Tsai, J.S., Li, S.J. and James Lee, L., 'Microstructural analysis of composite tubes made from braided preform and resin transfer molding', *J. Composite Mater.*, **32**(19), 829–850, 1998.
31. Marrey, R.V. and Sankar, B.V., 'A micromechanical model for textile composite plates', *J. Composite Mater.*, **31**(12), 1187–1213, 1997.
32. Witcomb, J. and Srirengan, K., 'Effect of various approximations on predicted progressive failure in plain weave composites', *Composite Structures*, **34**, 13–20, 1996.
33. Reddy, J.N., *An Introduction to the Finite Element Method*, McGraw-Hill, 1994.
34. Hibbitt, Karlsson and Sorensen, Abaqus Explicit Version 5.6, Abaqus Standard Version 5.6, User Manual, Inc. Pawtucket, RI.
35. Hull, D., *An Introduction to Composite Materials*, Cambridge University Press, Cambridge, 1981.
36. Zhu, H., Sankar, B.V. and Marrey, R.V., 'Evaluation of failure criteria for fiber composites using finite element micromechanics', *J. Composite Mater.*, **32**(8), 766–782, 1998.
37. Ramakrishna, S., 'Characterization and modeling of the tensile properties of plain weft-knit fabric reinforced composites', *Composites Sci. Technol.*, **57**, 1–22, 1997.
38. Rydin, R.W., Varelidis, P.C., Papaspyrides, C.D. and Karbari, V.M., 'Glass fabric vinyl–ester composites: tailoring the fiber bundle/matrix interphase with nylon coatings to modify energy absorption behavior', *J. Composite Mater.*, **31**(2), 182–209, 1997.
39. Frantziskonis, G.N., Karpur, P., Matikas, T.E., Krishnamurthy, S. and Jero, P.D., 'Fiber–matrix interface – information from experiments via simulation', *Composite Structures*, **29**(3), 231–248, 1993.
40. Gao, Z. and Reifsnider, K.L., 'Tensile failure of composites: influence of interface and matrix yielding', *J. Composites Technol. Res.*, **14**(4), 201–210, 1992.
41. Drzal, L.T. and Madhukar, M., 'Fibre–matrix adhesion and its relationship to composite mechanical properties', *J. Mater. Sci.*, 569–610, 1993.
42. De Moura, M.F.S.F., Gonçalves, J.P.M., Marques, A.T. and De Castro, P.M.S.T.,

'Modeling compression failure after low velocity impact on laminated composites using interface elements', *J. Composite Mater.*, **31**(15), 1463–1479, 1997.
43. Jayaraman, K., Reifsnider, K.L. and Swain, R.E., 'Elastic and thermal effects in the interphase: Part I. Comments on characterization methods', *J. Composites Technol. Res.*, **15**(1), 3–13, 1993.
44. Jayaraman, K., Reifsnider, K.L. and Swain, R.E., 'Elastic and thermal effects in the Interphase: II. Comments on modeling studies', *J. Composites Technol. Res.*, **15**(1), 14–22, 1993.
45. Effendi, R.F., Barrau, J.-J. and Guedra–De Georges, D., 'Failure mechanism analysis under compression loading of unidirectional carbon/epoxy composites using micromechanical modelling', *Composite Structures*, **31**(2), 87–98, 1995.
46. Muller, W.H. and Shmauder, 'Interface stresses in fiber-reinforced materials with regular fiber arrangements', *Composite Structures*, **24**(1), 1–22, 1993.
47. Naik, R.A. and Crews, J.H., Jr, 'Fracture mechanics analysis for various fiber/matrix interface loadings', *J. Composites Technol. Res.*, **14**(2), 80–85, 1992.
48. Mital, S.K. and Chamis, C.C., 'Fiber pushout test: a three-dimensional finite element computational simulation', *J. Composites Technol. Res.*, **13**(1), 14–21, 1991.
49. Drzal, L.T. and Madhukar, M., 'Measurement of fiber matrix adhesion and its relationship to composite mechanical properties', paper presented at the Eighth International Conference on Composite Materials, ICCM-8, Honolulu, 15–19 July, 1991.
50. Ebeling, T., Hiltner, A., Baer, E., Fraser, I.M. and Orton, M.L., 'Delamination failure of a woven glass fiber composite', *J. Composite Mater.*, **31**(13), 1319–1333, 1997.
51. Ebeling, T., Hiltner, A., Baer, E., Fraser, I.M. and Orton, M.L., 'Delamination failure of single yarn glass fiber composite', *J. Composite Mater.*, **31**(13), 1303–1317, 1997.
52. Drapier, S., Gardin, C., Grandidier, J.C. and Ferry M.P., 'Structure effect and microbuckling', *Composites Sci. Technol.*, **56**, 861–867, 1996.
53. Balacó De Morais, A.O. and Torres Marques, A., 'A micromechanical model for the prediction of the laminar longitudinal compression strength of composite laminates', *J. Composite Mater.*, **31**(14), 1397–1411, 1997.
54. Kyriakides, S. and Ruff, A.E., 'Aspects of the failure and postfailure of fiber composites in compression', *J. Composite Mater.*, **31**(20), 2000–2037, 1997.
55. Kelly, A. and Rabotnov, Yu.N., *Failure Mechanics Of Composites*, Handbook of Composites, Volume 3, North-Holland, 1985.
56. Brostow, W. and Corneliussen, R.D., *Failure of Plastics*, Hansen, 1986.
57. Hull, D., *Energy Absorbing Composite Structures: Scientific And Technical Review*, No. 3, pp. 23–30, University Of Wales, 1988.
58. Drechsler, K., Brandt, J., Larrodé, E., Miravete, A. and Castejón, L., 'Energy absorption behaviour of 3D woven sandwich structures', paper presented at 10th International Conference on Composite Materials, Vancouver, Canada, August, 1995.
59. Ivens, J., Verpoest, I. and Vandervleuten, P., 'Improving the skin peel strength of sandwich panels by using 3D-fabrics', *Proceedings of the ECCM*, vol. 5. Mathews, F.L., *et al.*, eds, Pergamon Press, London, 1987.

60. Miravete, A., Castejón, L. and Alba, J.J., 'Nuevas Tipologías de Fibra de Vidrio en Transportes', *Ibérica Actualidad Tecnológica*, **390**, 492–494, 1996.
61. Verpoest, I., Wevers, M., De Meester, P. and Declerrg, P., '2.5D and 3D-fabrics for delamination resistant composite laminates and sandwich structures', *Sampe J.*, **25**(3), 51–56, 1989.
62. Clemente, R., Miravete, A., Larrodé, E. and Castejón, L., *3-D Composite Sandwich Structures Applied to Car Manufacturing*, SAE Technical Papers Series, Detroit, MI, 1998.
63. Nakai, A., Fujita, A., Yokohama, A. and Hamada, H., 'Design methodology for a braided cylinder', *Composite Structures*, **32**, 501–509, 1995.
64. Chiu, C.H., Lu, C.K. and Wu, C.M., 'Crushing characteristics of 3-D braided composite square tubes', *J. Composite Mater.*, **31**(22), 2309–2327, 1997.
65. Karbhari, V.M., Falzon, P.J. and Herzerberg, I., 'Energy absorption characteristics of hybrid braided composite tubes', *J. Composite Mater.*, **31**(12), 1165–1185, 1997.
66. Cuartero, J., Larrodé, E., Castejón, L. and Clemente, R., *New Three Dimensional Composite Preforms and its Application on Automotion*, SAE Technical Papers Series, Detroit, MI, 1998.
67. Castejón, L., Cuartero, J., Clemente, R. and Larrodé, E., *Energy Absorption Capability of Composite Materials Applied to Automotive Crash Absorbers Design*, SAE Technical Papers Series, Detroit, MI, 1998.
68. Hill, R., *The Mathematical Theory of Plasticity*, Clarendon Press, Oxford, 1950.
69. Thornton, P.H. and Jeryan, R.A., 'Crash energy management in composite automotive structures', *Int. J. Impact Eng.*, **7**(2), 167–180, 1988.
70. Farley, G.L. and Jones, R.M., 'Crushing characteristics of continuous fiber-reinforced composite tubes', *J. Composite Mater.*, **26**(1), 1992.
71. Thornton, P.H., 'The crush behavior of glass fiber reinforced plastic sections', *Composites Sci. Technol.*, **27**, 199–224, 1986.